



© 1995-2026 by Isidoro Martínez

SPACECRAFT THERMAL MODELLING AND TESTING

Spacecraft thermal control. modelling and testing.....	1
STC goals and means.....	1
STC design procedure.....	3
Spacecraft thermal discretization.....	3
Preliminary thermal tasks.....	4
Spacecraft energy balance and thermal balance	5
Averaging radiation inputs.....	8
Global approach (the one spacecraft-node model)	9
Solar input.....	9
Steady temperature.....	10
Effect of thermo-optical properties	11
Effect of solar cells	12
Effect of satellite geometry	15
Effect of a sunshield.....	16
Effect of a concavity	16
Effect of planet: eclipse and own emission.....	17
Effect of planet: albedo	19
Analytical one-node sinusoidal solution	26
Two nodes models	29
Analytical two-nodes sinusoidal solution	35
Multi-node models	36
Node selection.....	36
Nodal equations.....	37
Node couplings	39
Numerical simulation.....	39
Analysis of results.....	41
Spacecraft thermal testing.....	42

SPACECRAFT THERMAL CONTROL. MODELLING AND TESTING

STC goals and means

It is well known that any kind of equipment is damaged if subjected to too-hot or too-cold an environment; the main goal of a [spacecraft thermal control \(STC\)](#) is to prevent overheating and undercooling in every part of equipment, at all phases of the [spacecraft mission](#) (mostly within the [space environment](#)).

The typical solution adopted in STC to avoid overheating (which cause permanent damage), is to choose cover materials with appropriate thermo-optical properties to keep the system basically cool, and to compensate the eventual undercooling (particularly at eclipses) by means of distributed electrical heaters. Undercooling, usually do not cause permanent damage but just a dormant non-operational state (which may be critical to the mission, however). Some over-dimensioning is always applied to cover contingencies. The problem with this simple solution is that electrical power is generally scarce in spacecraft (and more during

eclipse periods, when no solar power can be generated), what closely connects the STC system with the power management system (concerning battery capacity sizing).

The thermal control system (TCS) of internal items (e.g. electronic boxes) finally depends on the outer system boundaries. The final need may be:

- To reduce or increase the absorbed radiations from the environmental (sun, planet, other parts of the spacecraft). With an appropriate choice of solar-absorptance, α , and IR-emissivity, ε (really, just the α/ε ratio), for the external surfaces, it is easy to get steady temperatures from $-50\text{ }^{\circ}\text{C}$ to $150\text{ }^{\circ}\text{C}$ at Earth-Sun distances. The best to avoid thermal radiation absorption (and emission) is a multilayer insulation blanket ([MLI](#)).
- To reduce or increase heat losses to the environment. All active internal items dissipate. Batteries are the worst: they may dissipate $10^2..10^5\text{ W/m}^3$, and must always be maintained at about $0..30\text{ }^{\circ}\text{C}$ while charging (or $-10..50\text{ }^{\circ}\text{C}$ while discharging). Powerful microchips typically dissipate $10..20\text{ W/cm}^2$. Radiators are the primary TCS components for ultimate heat rejection; a second-surface mirror is a good radiator because it reflects a lot of solar radiation and emits a lot of infrared radiation (primary mirrors have low emissivity).
- To reduce or increase heat transfer between internal items, or keep them nearly isothermal (e.g. optical equipment). To bridge thermal expansion gaps, or to provide thermal switches. External elements like solar arrays and antennas are nearly isolated from the main body.
- Thermal control technologies may be classified in accordance with the thermal path: heat sources, heat storage, heat transportation, heat rejection (but energy is not always flowing downward the temperature scale; e.g. thermo-electric coolers), etc.

It should be mentioned that, besides the thermal loads, TCS equipment must withstand mechanical and chemical loads; e.g. particle impacts, particularly across micrometeoroid belts (e.g. towards GEO or deeper space). MLI blankets provide some protection against cosmic dust and some micro-meteoroid impacts.

Classical TCS are based on radiative energy emission from the spacecraft envelop (the total hemispherical emissive power-density of a black-body is $M_{bb}=\sigma T^4$), usually concentrated on some surfaces specifically designed for the purpose of heat rejection (radiators), with some metal conduction along cold plates from equipment inside. In modern TCS, however, two-phase technologies have become the standard tools for spacecraft thermal control: heat pipes and loop heat pipes, micro electromechanic (MEMS) two-phase fluid loops, phase-change materials (PCM), heat pumps, cryogenics...

Liquid evaporation and solid ablation are the most efficient cooling means, but rarely used because of the mass penalty: water droplet evaporation was used on the Shuttle during take-off and landing (where the radiators were not working), water ice sublimation is used to cool space suits during extravehicular activity (EVA), and ablation is used in all re-entry probes and vehicles other than the re-usable Shuttle.

STC design procedure

There is a great variety of actions related to a given spacecraft thermal control project. The traditional steps followed in the thermal design of a spacecraft may be (in chronological order):

- Identify your components (at least the most sensitive items) within the overall system:
 - Identify spacecraft geometry and dimensions. Compile data of similar systems (missions, platforms, and payload details).
 - Identify component data: geometry and dimensions, mass and thermal capacity, thermal conductivity of materials and joints, and surface thermo-optical properties.
 - Identify thermal requirements from mission and operation data (e.g. power dissipation laws).
- Perform a thermal analysis to find the expected temperature field and evolution:
 - Identify thermal environment inputs and outputs, and heat paths between elements.
 - Assume default values for unspecified characteristics, from previous experience (e.g. properties for passive thermal control technologies).
 - Identify thermal worst cases.
 - Make a thermal mathematical model (TMM) for parametric simulation. At first stages in the design, a crude analytical model may be appropriate (geometrical and material details may not be available), but most of the times, a detailed numerical model must be developed.
 - Check your solution for consistency (by energy balances, by limit values, by sensitivity to parameter changes...).
- Propose a suitable design:
 - Propose a basic solution to be integrated in the current overall spacecraft design: radiator sizing and design, heaters, mass and power budgets, and special STC items.
 - Propose enhancements to the basic solution, identifying interactions of STC with other subsystems.
 - Iterate with new inputs from the other subsystems, and propose solutions to new problems (with the corresponding analysis that supports it).
- Assure the design:
 - Propose on-board thermal control diagnostics to monitor proper operation during tests and flight operations. Plan to detect abnormal behaviour.
 - Verify predictions with tests, and refine the design if needed (an iterative process).

Spacecraft thermal discretization

The modelling approach in STC can be, in what concerns the space, time, and parameter discretization, continuous (for simple analytical models), discretized in a spatial network of nodes and node couplings, or statistical in nature (as for the Monte Carlo ray-tracing method used to compute radiative exchanges).

Heat-transfer problems with non-trivial geometries are too complicated for analytical study, and one has to resort to numerical simulation, with space and time discretization along the following steps:

- First, the spacecraft geometry must be defined, even if as a crude mock-up at early stages in design. A modular conception (subsystems and payloads) helps on the future refining process.
- Then the geometry is discretized, dividing the system into small pieces or lumps which, in the finite difference method (FDM) are considered isothermal and represented by just one material

point, the node, and in the finite element method (FEM) are considered having a linear temperature field and represented by a few corner nodes. Additional nodes are usually added to represent the background environment, although for manual modelling they are usually considered apart. It is important to remember that a finer mesh will not improve accuracy beyond uncertainties in other data (e.g. thermo-optical coefficients).

- Then the energy balance equation for each node is established, with the thermal capacity, heat dissipation and background loads ascribed to the node, and with the appropriate heat transfer couplings with the other nodes.
- Time discretization provides a step-by-step updating temperature matrix, in terms of some initial conditions (maybe difficult to know) and the boundary conditions applied; a case study (trajectory and operations, must be specified. Boundary conditions are changing all the time, so, only representative situations are studied, but at least the worst hot case (maximum power and heat fluxes at end of life, EOL), and worst cold case (minimum power and heat fluxes at beginning of life, BOL), must be studied.
- Assign particular power-dissipation profiles to each node (they may depend on eclipse timing, and unknown operations).
- Ascribe thermal-connection properties to node pairs: conductance factors to adjacent nodes, radiation factors to field-of-view nodes, and convection coefficients to internal fluid media, if any. This task is independent of spacecraft trajectory for fixed-geometry spacecraft, but it is coupled to orbit and attitude motion when there are some deployed or pointing elements with relative motion to the spacecraft body.
 - Conductance couplings only depend on contact area between adjacent nodes and thermal conductivities of materials.
 - Radiation couplings depend on thermo-optical properties of surfaces, and viewing factors.
- After this lengthy preparatory work, the system of local energy balances is solved for the node temperatures.
- The output of the solver is visualized with appropriate computer-graphics tools, and extreme values automatically sorted.

Preliminary thermal tasks

Before any meaningful spacecraft thermal control design is attempted, there is a variety of tasks for the thermal engineers. From the simpler to more complex tasks, a list may be:

- Find some specific material properties, e.g. thermal conductivity of a given composite material, or the freezing point of an on board propellant (e.g. [hydrazine](#)).
- Solve simple heat-conduction problems, e.g. find the heat flow through a conical support between isothermal surfaces. Notice that the design goal may be varied (exemplified here with this planar and steady thermal-conduction problem), e.g.:
 - $\dot{Q} = kA(T_1 - T_2)/L$, i.e. find the heat flux for a given set-up and T -field.
 - $T_1 = T_2 + \dot{Q}L/(kA)$, i.e. find the temperature corresponding to a given heat flux and set-up. Notice that our thermal sense (part of the touch sense) works more along balancing the heat flux than measuring the contact temperature, what depends on thermal conductivity of the

- object; that is why Galileo masterly stated that we should ascribe the same temperature to different objects standing in a room, like wood, metal, or stone, contrary to our sense feeling.
- $k = \dot{Q}L / (A\Delta T)$, i.e. find an appropriate material that allows a prescribed heat flux with a given T -field in a given geometry.
 - $L = kA(T_1 - T_2) / \dot{Q}$, i.e. find the thickness of insulation to achieve a certain heat flux with a given T -field in a prescribed geometry.
 - Solve simple thermal relaxation problems, e.g. find the heat-up time after powering some device.
 - Solve simple thermo-hydraulic problems, e.g. find the pumping power for a given fluid loop duty, or the Nusselt number dependence on Reynolds number.
 - Solve simple thermal-radiation problems, e.g. find the heat dissipation in a louver as a function of tilting, or the radiative coupling between a solar panel and a planet.
 - Solve simple thermal balance problems, e.g. find the steady temperature of an isothermal body in space as a function of orbit phase and attitude.
 - Solve more complex thermal problems, e.g. find the steady temperature field (basically the extreme temperatures) in a conductive shell in space, for different geometries, material properties, and external loads.
 - Solve full spacecraft thermal problems, e.g. accounting for transitories in power dissipation and thermal loads from the environment, variable geometries, etc.

SPACECRAFT ENERGY BALANCE AND THERMAL BALANCE

In the case of STC, it is often assumed that the mass of the system under study is invariant, either when considering the whole spacecraft or the smallest piece of equipment (e.g. propellant flow rates are not considered in thermal studies), so that the energy balance is that of a closed system, $dE/dt = \dot{W} + \dot{Q}$, where energy store is basically due to temperature change, $dE/dt = mcdT/dt$, though other types of energy store may be important (e.g. electrical store in batteries and condensers, thermal store in phase change materials, or other physic-chemical or nuclear modes of energy storage). The full open-system energy balance, $dE/dt = \dot{W} + \dot{Q} + \sum h_{in-out} \dot{m}_{in-out}$ (where \dot{m}_{in-out} are the mass flow-rates at the system frontier, and h_{in-out} their enthalpie), is required to analyse thermal protection systems based on ablative processes (where mass is lost), and to analyse TCS with fluid flow, as in fluid loops, heat pipes, cryocooling, sublimators...

The flow rate of work, \dot{W} (through the system frontier), may be an electrical input or output through umbilicals (e.g. heaters and solar cells), an electromagnetic input or output (solar cells, lasers, antennas), a mechanical input or output (e.g. by friction), etc. The flow rate of heat, \dot{Q} (through the system frontier), is always due to a temperature difference, and is traditionally split into conduction, convection, and radiation, the latter being the most complex and genuine effect in space thermal control.

As most spacecraft incorporate photovoltaic cells, it is worth considering the following energy balance applicable to the whole spacecraft or to a piece of equipment, with thermal, electrical, and electromagnetic energy terms:

$$\frac{dE}{dt} = \dot{W}_{\text{net}} + \dot{Q}_{\text{net}} = \frac{dE_{\text{th}}}{dt} + \frac{dE_{\text{ele}}}{dt} = \dot{W}_{\text{em,net}} + \dot{W}_{\text{ele,net}} + \dot{Q}_{\text{cond,net}} + \dot{Q}_{\text{conv,net}} + \dot{Q}_{\text{rad,net}} \quad (1)$$

where only two types of internal energy storage are considered: thermal, E_{th} , and electrical, E_{ele} (but not nuclear or mechanical storage); only two types of work flow are considered: $\dot{W}_{\text{em,net}}$, i.e. electromagnetic radiation (e.g. solar radiation, laser, or microwave radio-link, but not infrared, which is accounted as a heat flow), and $\dot{W}_{\text{ele,net}}$, i.e. electrical currents (through wires); finally, the three classical heat flow types are considered in (1): conduction through solids, fluid convection, and radiation. Notice that we here include solar radiation in the work term, as if it come from a large laser, in spite that of it being almost a perfect blackbody; the reason is that we intend to restrict our analysis of radiation heat transfer to thermal sources in the far infrared band of the EM-spectrum, leaving thermal sources in the visible and near-IR (the Sun), and non-thermal sources in any band (lasers in the visible or the infrared, microwaves, X-rays...) as work exchanges (independent on the system temperature).

Thermal energy storage may be due to a temperature change or to a phase change; if the latter is excluded (but notice that phase-change materials are sometimes used not only to increase thermal inertia but to drive thermal switches), then $dE_{\text{th}}/dt = CdT/dt$, where $C = \Sigma mc$ is the overall thermal capacity of the element.

Electrical energy storage depends on the state of charge (SOC) of batteries (and electrical capacitors, if relevant). There are several methods to measure SOC, but none is perfect. The simplest is the voltage method, but it is only precise near full load or empty states, and it has to be complemented with the coulomb-counting method. The voltage method is based on the dependence of the supply voltage, V , with SOC; it is a decreasing function (in the shape of a lying-down \int) that depends also on the operating temperature, T , and current being drawn I ; i.e. $V = V(\text{SOC}, T, I)$. The coulomb-counting method (or current-integration method) is based on knowing an initial SOC (usually fully loaded), and integrating the drawn current, $\int Idt = dQ$ (Q is here the electrical charge), what yields the SOC approximately, since some of the charge is converted to heat by internal leakage current. Neglecting this latter effect (which can be accounted for if the battery efficiency is known), the electrical energy storage can be approximated as $dE_{\text{ele}}/dt = VdQ/dt$, where V is the nominal voltage and Q the battery capacity (equivalent to a condenser electrical charge available to do work, electrochemical work in the case of batteries); maximum battery capacity, Q_{max} , is commonly given in A·h (1 Ah=3600 C), and $\text{SOC} \equiv Q/Q_{\text{max}}$, most often stated in percentage. Full-load energy stored is $V \cdot Q$ (e.g. a small battery pack of 4 kg for a 50 kg educational satellite may have 25 Ah at 24 V, i.e. it accumulates $E_{\text{ele,max}} = Q_{\text{max}}V = 25 \cdot 24 \cdot 3600 = 2.2 \text{ MJ} = 0.6 \text{ kWh}$).

The total energy balance (1) may be split into an electrical energy balance (including EM terms because we really want them to split in work and heat terms), and a thermal energy balance, although some source and sink energy terms must be introduced, since only total energy is conservative:

$$V \frac{dQ_{\text{ele}}}{dt} = (\dot{W}_{\text{em,in}} - \dot{W}_{\text{em,out}} - \dot{W}_{\text{em,dis}}) + (\dot{W}_{\text{ele,in}} - \dot{W}_{\text{ele,out}} - \dot{W}_{\text{ele,dis}}) \quad (2)$$

$$C \frac{dT}{dt} = \dot{W}_{\text{em,dis}} + \dot{W}_{\text{ele,dis}} + \dot{Q}_{\text{cond,net}} + \dot{Q}_{\text{conv,net}} + \dot{Q}_{\text{rad,net}} \quad (3)$$

where Q_{ele} is the actual battery charge capacity, $\dot{W}_{\text{em,dis}}$ is the dissipated direct-beam electromagnetic radiation, and $\dot{W}_{\text{ele,dis}}$ is the dissipated electrical power, both contributing to heating (temperature increase), and which are traditionally quoted as dissipated ‘heat’, $\dot{Q}_{\text{em,dis}}$ and $\dot{Q}_{\text{ele,dis}}$ (but recall that what enters to a resistor is electrical work, not heat). Thermal terms in (3) are typically one order of magnitude larger than electrical terms (electrical efficiency of solar cells is low), and this is the reason why the energy balance is often reduced to a thermal balance to a first approximation.

Notice again that, with the two-band radiation model introduced in [Heat transfer and thermal radiation modelling](#), radiation in the infrared band is accounted as heat and modelled as $\dot{Q}_{\text{rad}} = \sigma R_{12} (T_1^4 - T_2^4)$, whereas radiation in the solar band is accounted as work (because it is at a much higher temperature than that of the object) and modelled as $\dot{W}_{\text{em}} = \alpha EA_{\text{frontal}}$, where α is the absorptance of the object to solar radiation, and E is the frontal irradiance, as explained below (it is not accounted as heat because it is not a ‘temperature-difference’ term).

For the typical case of thermal control of a satellite in orbit around a planet, the different energy inputs from the space environment (Fig. 1) may be:

- Solar radiation (always understood as direct sunshine). Surface absorptance marks the fraction of incident radiation absorbed, usually heating the system, although a part may go out as generated electricity in solar cells.
- Planetary albedo (solar reflection on a nearby planet or moon). Same effects as for direct solar radiation.
- Planetary emission. Far-infrared radiation coming from a nearby planet or moon.
- Reflected solar radiation from other parts in our spacecraft (e.g. solar panels, antenna, optical shrouds, deployed radiators...).
- Reflected solar radiation from nearby spacecraft (e.g. a spacecraft approaching a space station), although this is usually a small transient phase irrelevant to thermal control.
- Other ‘monochromatic’ radiations absorbed by the satellite (microwaves, X-rays...) are negligible in all common cases.

As for the radiation output, if only the absorbed solar radiation (direct and albedo) is contemplated in the energy balance (not the total incident solar power), the only non-heat radiations emitted by a satellite are those used for communications (microwaves and lasers, including IR-lasers), since all the thermal radiations in the far-infrared band can be modelled as heat transfer terms with the background sky at 2.7 K, with the planet or moon in the surroundings, or with nearby spacecraft parts. Notice that another approach to deal with planet emission may be to account only for the absorbed part on the satellite surface, and then consider the surface emission to the whole 2π steradians; the difference is negligible because the planet size is much larger, and because inputs from the 2.7 K source are negligible.

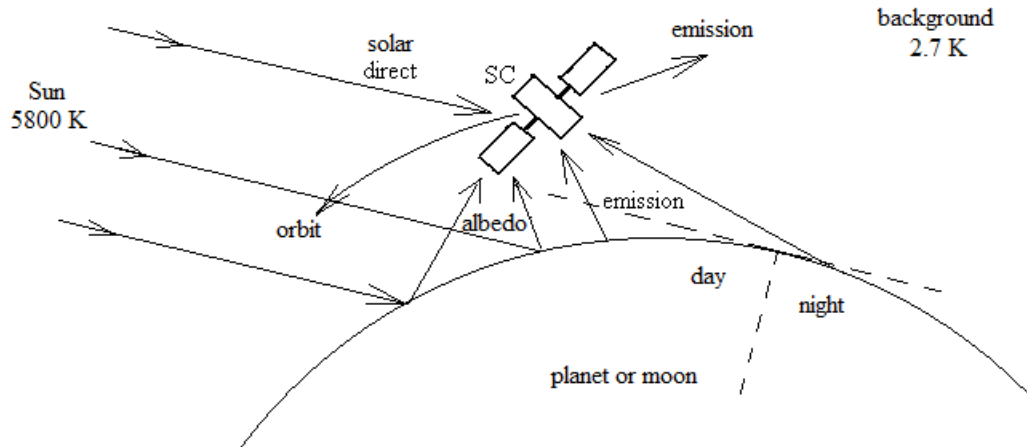


Fig. 1. Typical thermal control configuration: a spacecraft (SC) orbiting a planet or moon, from which albedo and planet emission may be important energy inputs, besides direct sunshine; spacecraft emission to the background space, at 2.7 K, is always important.

To analyse in detail all the terms in the energy balance, it is better to start from a global approach and consider a complete spacecraft, before entering into the details of thermal balances for subsystems and elements. In any case, but particularly for global analysis, radiation characteristics (thermo-optical properties, planet properties, and other heat inputs) are averaged to simplify the problem.

Averaging radiation inputs

For planetary orbits, the three bodies Sun-planet-spacecraft are moving relative to each other along orbits that are described parametrically in terms of time. And it is not just a three points system but a three-solid system with rotational motions beside their translation motion. And spacecraft geometry may change with time due to mission requirements, notably solar panels, antennas, and radiators. And some of the time variations are unpredictable, the best example is albedo contribution from cloud coverage on Earth.

Fortunately, thermal inertia of spacecraft parts act as a bass-pass filter that averages most of the thermal response to such rapidly changing scenario. For instance, a polar-LEO satellite may be exposed to big changes in radiation input when going from the Equator to the Poles in less than 25 minutes (96 minutes polar orbit): local Earth albedo may change from $\rho=0.05$ over uncloudy regions of tropical oceans to $\rho=0.90$ over the Antarctic, and Earth IR emission too, with surface temperatures over 300 K over tropical lands to under 200 K over Antarctica. But these big changes have little influence on the thermal balance of the satellite, and only the most lightweight and decoupled spacecraft elements may follow such swift changes.

It is customary in STC to use planet averaged properties (one representative temperature, constant albedo, and constant emissivity), and sometimes orbit averaged values for external and internal heat loads. When instantaneous values are computed, one usually understands 'instantaneous' to mean 'several-minutes averaging'.

Global approach (the one spacecraft-node model)

Solar input

As explained under [Space environment](#), solar energy impinging on a spacecraft can be approximated by a parallel beam irradiance, E , with a value at the standard Sun-Earth distance (i.e. the astronomical unit [ua], or AU; 1 ua=150·10⁹ m) of $E=1360$ W/m² (known as ‘the solar constant’, sometimes named C_s), and with a spectral distribution corresponding to a blackbody at 5800 K.

Solar input on a spacecraft element may be difficult to calculate for complex geometries when shadows are cast from other parts, semi-transparent parts are interposed, or solar incident angles vary from point to point. We assume for the moment that all solar absorption is dissipated and heats the system, analysing later the case of solar cells. The easiest case to analyse is one side (recall that each face must be separately considered in radiative exchanges), of an opaque planar element (which becomes the generic case when surface discretization renders small patches quasi-planar), whose normal direction is tilted an angle $\beta \in [0, \pi/2]$ from the Sun direction. A fraction of the incident solar energy is reflected and the rest is absorbed at the surface (within the first millimetre really) being totally dissipated and causing a heating effect equivalent to a ‘solar heat’ input:

$$\dot{Q}_s = \alpha EA_{\text{frontal}} = \alpha EA \cos \beta \quad \text{for } |\beta| \leq \pi/2, \quad \dot{Q}_s = 0 \quad \text{otherwise} \quad (4)$$

i.e. solar input is proportional to surface absorptance, α ($\alpha=1$ for a black-body), solar irradiance, E ($E=1360$ W/m² at 1 ua, decreasing with the square of the distance to the Sun), and surface projected area in the Sun direction, A_{frontal} ,

The collimated solar radiation can be applied to all solar planet flybys (Mercury orbit at perihelion distance is $R_{\text{sp}}=0.31$; 0.1 ua is equivalent to 10 Sun diameters); otherwise, the view factor approach can be always followed (e.g. a frontal planar surface of area A at a distance H from the centre of a sphere of radius R , radiating as a blackbody at temperature T_s , gets a power $\dot{Q}_s = \alpha AF_{12} \sigma T_s^4$, with $F_{12}=(R/H)^2$; see [View factor tabulations](#)).

The simplest thermal model for a spacecraft may be an isothermal spherical mass under vacuum, exposed to sunshine, without solar cells and far from any planet influence. Its thermal balance (3) can be written as:

$$C \frac{dT}{dt} = \dot{W}_{s,\text{dis}} + \dot{W}_{\text{ele},\text{dis}} - \dot{Q}_{\text{out}} = \alpha EA_{\text{frontal}} + \dot{Q}_{\text{ele},\text{dis}} - \varepsilon A \sigma T^4 \quad (5)$$

where C is the overall thermal capacity ($C=\Sigma mc$, with typical values of $c=1000$ J/(kg·K)), $T(t)$ is the temperature evolution sought, $\dot{W}_{s,\text{dis}} = \dot{Q}_s = \alpha EA_{\text{frontal}}$ is the heating by absorption and dissipation of direct solar radiation (the only EM radiation input considered), $\dot{W}_{\text{ele},\text{dis}} = \dot{Q}_{\text{ele},\text{dis}}$ is the electrical power dissipated during its operation (e.g. from ground-loaded batteries, like in Sputnik), ε is the average emissivity of surfaces in the far-infrared range (recall that $\alpha \neq \varepsilon$ for different radiation bands), A is the whole emitting area (assumed without concavities), and $\sigma=5.67 \cdot 10^{-8}$ W/(m²·K⁴) is the Stefan-Boltzmann constant. Notice that

we have used $\dot{Q}_{\text{out}} = \varepsilon A \sigma T^4$ instead of the proper heat radiation transfer $\dot{Q}_{\text{out}} = \varepsilon A \sigma (T^4 - T_{\infty}^4)$, neglecting the small contribution from the cosmic background radiation temperature, $T_{\infty}=2.7$ K, and that a parallel solar beam was assumed. Finally notice that a passive object (without $\dot{Q}_{\text{ele,dis}}$) under permanent solar eclipse by a distant celestial body, would tend to equilibrate with background radiation at 2.7 K (this configuration can be advantageously used to keep a spacecraft at cryogenic temperatures, as has been done with the Herschel and Planck, and is intended for the James Webb Space Telescope, although the eclipse is not total in practice because Earth's umbra cone only extends to $1.4 \cdot 10^9$ m and the Sun-Earth libration point is at $1.5 \cdot 10^9$ m; besides, the spacecraft usually follow Lissajous orbits around those points, so that solar panels are still used to power them).

Steady temperature

If the solar input does not depend on time, and the dissipation term is neglected, then the temperature attains a steady value (often called 'equilibrium' temperature) given by:

$$0 = \alpha E A_{\text{frontal}} - \varepsilon A \sigma T^4 = \alpha E \pi R^2 - \varepsilon 4 \pi R^2 \sigma T^4 \rightarrow T = \left(\frac{\alpha E}{4 \varepsilon \sigma} \right)^{\frac{1}{4}} \quad (6)$$

which can be set in terms of the Sun temperature ($T_s=5800$ K), Sun radius ($R_s=0.70 \cdot 10^9$ m), and Sun-to-probe distance, $R_{s,p}$, when substituting E :

$$E = \sigma T_s^4 \frac{4 \pi R_s^2}{4 \pi R_{s,p}^2} \rightarrow T = T_s \sqrt{\frac{R_s}{2 R_{s,p}}} \quad (7)$$

Exercise 1. Consider the variation of solar irradiance with distance to the Sun. Find:

- The solar irradiance and the steady temperature for a spherical black-body at the distance of each of the 8 planets, and compare with their mean surface temperature.
- Find the solar irradiance change at Earth's perihelion and aphelion, and the steady temperature variation for a spherical blackbody.
- Find the solar irradiance and the steady temperature for a spherical blackbody at 0.28 ua (the expected perihelion of Solar Orbiter spacecraft).

Sol.:

- The solar irradiance and the steady temperature for a spherical black-body at the distance of each of the 8 planets, and compare with their mean surface temperature.

Irradiation decreases with distance squared, as stated in Eq. (7). With the mean extra-terrestrial solar irradiance, $E=1360$ W/m², and the data for mean radius for planet orbits, $R[\text{Mercury, Venus, Earth, Mars, Jupiter, Saturn, Uranus, Neptune}]=[0.38,0.72,1,1.52,5.19,9.51,19,30]$ ua, working in astronomical units ua ($1 \text{ ua}=150 \cdot 10^9$ m), we build Fig. E1, where the real mean surface temperature for the planets, $T[\text{Mercury, Venus, Earth, Mars, Jupiter, Saturn, Uranus, Neptune}]=[435,733,288,217,102,63,57,57]$ K, have been marked for comparison.

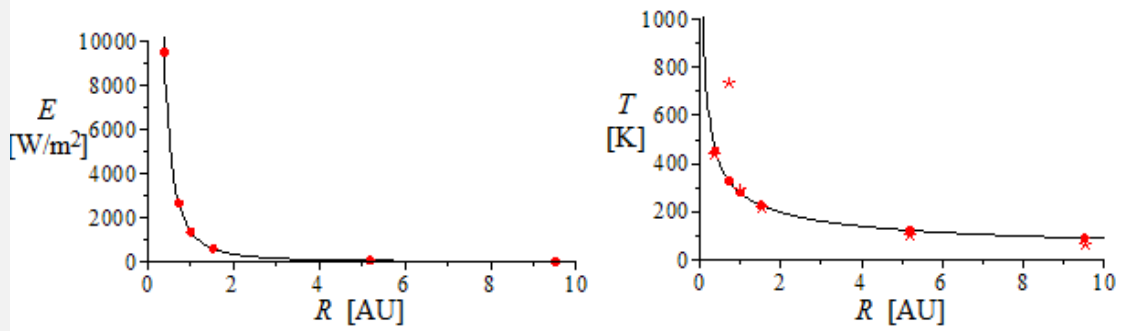


Fig. E1. Variation of solar irradiation and the steady temperature of a blackbody with distance to the Sun. Comparison with real mean surface temperature for the planets.

Notice how Venus real surface temperature (733 K) departs from blackbody calculations (329 K), due to the large greenhouse effect there.

- b) Find the solar irradiance change at Earth's perihelion and aphelion, and the steady temperature variation for a spherical blackbody.

Earth's orbit eccentricity is $e=0.0167$, so that, near 1 ua, $E=E_0(R_{s-e}/R_{s-e,0})^2=E_0(1\pm e)^2\approx E_0(1\pm 2e)=1360\cdot(1\pm 2\cdot 0.0167)=1360\pm 46$ W/m². The steady temperature variation for a spherical blackbody is $T_{st}=[E/(4\sigma)]^{1/4}=[E_0(1\pm 2e)/(4\sigma)]^{1/4}=T_{st,0}(1\pm e/2)=279\pm 2.3$ K. Notice that a change of 1 W/m² in E , yields a change of 0.05 °C in T_{st} .

- c) Find the solar irradiation and the steady temperature for a spherical blackbody at 0.28 ua (the expected perihelion of Solar Orbiter spacecraft),

At 0.28 ua, $E_{0,23}=E_1(1/0.28)^2=1360\cdot 13=17.5$ kW/m². The steady energy balance for a spherical black-body is $0=\dot{Q}_{solar}-\dot{Q}_{space}=EA_{frontal}-A\sigma T^4=E\pi R^2-4\pi R^2\sigma T^4$, and thus $T=(E/(4\sigma))^{1/4}=(17500/(4\cdot 5.67\cdot 10^{-8}))^{1/4}=527$ K (254 °C). Notice that the collimated beam model has been used, in spite of the closeness of the Sun.

Effect of thermo-optical properties

The easiest and cheapest method of thermal regulation in space is based on selecting surface finishing with [appropriate thermo-optical properties; representative values](#) can be found aside for the two-spectral-band model (explained in [Heat transfer and thermal modelling](#)).

Exercise 2. Find the steady temperature for an isothermal sphere at geosynchronous orbit, neglecting Earth interactions, as a function of surface absorptance divided by surface emissivity, with application to a blackbody ($\alpha/\varepsilon=1/1$), a white painting with $\alpha/\varepsilon=0.20/0.85$, a black painting with $\alpha/\varepsilon=0.95/0.90$, an aluminised painting with $\alpha/\varepsilon=0.30/0.30$, a golden painting with $\alpha/\varepsilon=0.25/0.03$, and a second surface mirror with $\alpha/\varepsilon=0.08/0.80$.

Sol.: From the energy balance at the steady state, $0=\dot{Q}_{solar}-\dot{Q}_{space}=\alpha EA_{frontal}-\varepsilon A\sigma T_{st}^4=\alpha E\pi R^2-\varepsilon 4\pi R^2\sigma T_{st}^4$, one gets for the steady temperature of an isothermal sphere, $T_{st}=[\alpha E/(4\varepsilon\sigma)]^{1/4}$, which is plotted in Fig. E2 as a function of the ratio α/ε .

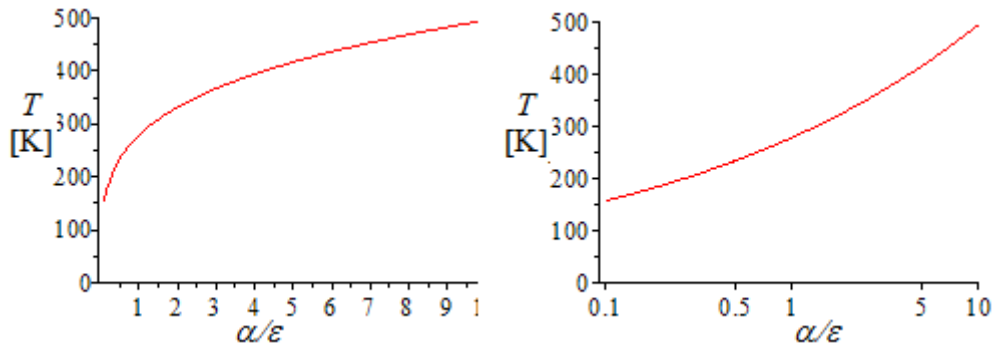


Fig. E2. Variation of the steady temperature of an isothermal sphere with the ratio α/ϵ .

For the different surface properties stated, the general solution, $T_{st}=[\alpha E/(4\epsilon\sigma)]^{1/4}$, takes the following values: $T_{st,bb}=279$ K, $T_{st,white}=193$ K, $T_{st,black}=282$ K, $T_{st,alum}=275$ K, $T_{st,gold}=472$ K, $T_{st,\alpha=0.7}=255$ K, and $T_{st,\alpha=0.7,\epsilon=0.6}=288$ K. Notice how hot is the golden paint, and how cold is the second surface mirrors (SSM, also known as optical solar reflectors, OSR), which are widely used for radiators in space, which are made of a transparent layer (e.g. a 0.25 mm fused-quartz plate, or a Teflon film), metallised on the back with silver or aluminium, and bonded to a substrate support.

Effect of solar cells

The first solar-powered satellite was Vanguard-1, in Mar-1958 (the 4th satellite ever launched, after Sputnik 1 in Oct-1957, Sputnik 2 in Nov-1957, and Explorer 1 in Jan-1958), shortly after the [first practical photovoltaic cell](#) was publicly demonstrated on 25 April 1954 at Bell Laboratories.

Most spacecraft get their electrical power from photovoltaic solar panels (wall-mounted or deployed), because, in spite of their high first cost, they are the most efficient in terms of power/mass ratio, and the most reliable (no moving parts, wide operating temperature range, no need of cooling...). The reason to deal with them here, at this elementary stage in spacecraft thermal modelling, is the confusion that may arise between solar heating and electrical dissipation in energy balances like in Eq. (5).

The main goal of solar cells is to produce electricity from sunshine, and the radiation-to-electricity energy efficiency is the ratio of the maximum power produced at 25 °C, $\dot{W}_{max}=(VI)_{max}$, divided by the standard input irradiance, E , and surface area, A , i.e.:

$$\eta \equiv \frac{(VI)_{max}}{EA} \quad (8)$$

where the standard for space applications is mean extra-terrestrial irradiance, $E=1360$ W/m² (also named as AM0 or air-mass-zero conditions) and the standard for ground applications is mean surface solar irradiance with 1.5 times the mean vertical clean air mass filter, $E=1000$ W/m² (also named as AM1.5 or air-mass-one-point-five conditions). Typical efficiencies of space-qualified silicon solar cells (at AM0, in vacuum) are $\eta=0.15..0.20$ (15..20%), but modern triple-junction GaAs cells reach $\eta=0.3$ (30%). For solar panels, i.e. assemblies of solar cells connected in series and parallel to have a certain voltage and intensity, a packaging factor, F_{pg} , is introduced to account for the effective cell area relative to the panel area to be

used in (8), which includes the collector wirings and other connections; a typical value is $F_{pg}=0.8$). Solar cell efficiency decreases with temperature, typically some 0.04%/K (e.g. if it is $\eta=25\%$ at 25 °C, it falls to $\eta=23\%$ at 75 °C, the typical operating temperature of deployed solar panels in low Earth orbit).

Solar cells should be facing solar radiation for maximum output, but this is not always possible. On small spacecraft, solar panels are fixed to the body, which may be spinning for attitude stabilization and thermal-control homogenization. Larger spacecraft have detached solar panels, with the main body maintained permanently oriented towards the Earth (for observation and/or communications) and the solar wings oriented towards the Sun as much as possible; for an orbiting spacecraft, a deployed solar panel revolves around its axis 360°/orbit (the so-called alpha-gimbal). Besides, on larger spacecraft like the ISS, a secondary rotation (the so-called beta-gimbal) slowly rotates to match the orbit solar angle, β (or just [beta angle](#), i.e. the angle from sunshine direction to the orbit plane); in the ISS, this is a two-month-period oscillation with some 100° amplitude side-to-side.

The electrical balance (really the non-thermal balance (2), including electromagnetic radiation outside the far IR band, electrical energy, mechanical energy...), for a solar panel can be reduced to:

$$\begin{aligned} \frac{dE_{\text{ele}}}{dt} &= \begin{pmatrix} \dot{W}_{\text{em,in}} - \dot{W}_{\text{em,out}} - \dot{W}_{\text{em,dis}} \\ \alpha EA_{\text{frontal}} & 0 & 0 \end{pmatrix} + \begin{pmatrix} \dot{W}_{\text{ele,in}} - \dot{W}_{\text{ele,out}} - \dot{W}_{\text{ele,dis}} \\ 0 & \eta F_{\text{pg}} EA_{\text{frontal}} & 0 \end{pmatrix} \\ \rightarrow \dot{W}_{\text{em,dis}} = \dot{Q}_s &= (\alpha - \eta F_{\text{pg}}) EA_{\text{frontal}} = \alpha_{\text{th}} EA_{\text{frontal}} \end{aligned} \quad (9)$$

i.e., the electromagnetic dissipation or ‘solar heat’ is an effective thermal absorptance, α_{th} , times irradiance times frontal area, since accumulation dE_{ele} and dissipation \dot{W}_{dis} can be neglected in the panels (and there is no electrical input or electromagnetic output). Notice that solar absorptance α in (9), due to the photovoltaic semiconductor material (the protective cover glass, some 0.1 mm thin, is almost transparent to solar radiation), is defined in terms of reflectance ρ as $\alpha=1-\rho$, a measure independent of actual electric yield. Solar cell emissivity is dependent on the type of protective cover glass, with typical values in the range $\varepsilon=0.7..0.9$.

However, if a global approach is followed and one selects the total system, including the solar panels, the electrical consumers, and the batteries, the electrical balance becomes:

$$\begin{aligned} \frac{dE_{\text{ele}}}{dt} &= \begin{pmatrix} \dot{W}_{\text{em,in}} - \dot{W}_{\text{em,out}} - \dot{W}_{\text{em,dis}} \\ \alpha EA_{\text{frontal}} & 0 & \alpha_{\text{th}} EA_{\text{frontal}} \end{pmatrix} + \begin{pmatrix} \dot{W}_{\text{ele,in}} - \dot{W}_{\text{ele,out}} - \dot{W}_{\text{ele,dis}} \\ 0 & 0 & 0 \end{pmatrix} \\ \rightarrow \frac{dE_{\text{ele}}}{dt} &= \eta F_{\text{pg}} EA_{\text{frontal}} - \dot{W}_{\text{ele,dis}} \end{aligned} \quad (10)$$

showing that the accumulation in batteries compensates the electrical production ($\eta F_{\text{pg}} EA_{\text{frontal}}$) with the electrical consumption, $\dot{W}_{\text{ele,dis}}$ (given by the operational procedures). The batteries themselves must be taken as consumers too, since they typically dissipate up to 10% of delivery power. Notice that if the solar

cells are in open circuit (producing no power) all the terms in the electrical balance are null, and all the absorption goes to heating, $\alpha = \alpha_{th}$.

The thermal balance (3) for a solar panel takes then the same form as for the whole spacecraft (in each case with their appropriate values, of course):

$$C \frac{dT}{dt} = \dot{W}_{em,dis} + \dot{W}_{ele,dis} + \dot{Q}_{cond,net} + \dot{Q}_{conv,net} + \dot{Q}_{rad,net} = \alpha_{th} EA_{frontal} + \dot{Q}_{ele,dis} - \varepsilon A \sigma T^4 \quad (11)$$

showing that the operational details for electricity consumption (the ‘electrical heat’), $\dot{Q}_{ele,dis}(t)$, must be known to solve the global energy balance (a crude first-order approximation is to consider $\dot{Q}_{ele,dis} = \text{constant}$ (equal to the mean electrical production of the solar panels)).

Exercise 3. Find the electrical power produced by an spherical satellite of 0.5 m in diameter, fully covered by solar cells of an efficiency $\eta = 15\%$ and a packaging factor $F_{pg} = 0.8$, in a low Earth orbit without eclipses, and set the thermal balance, assuming an absorptance and emissivity of $\alpha = \varepsilon = 0.75$ for the solar cells, a thermal capacity of $C = 30$ kJ/K for the satellite, and that the electrical dissipation is only important during 15 minutes of the orbit, and can be considered constant in that period.

Sol.: The solar panel produce $\dot{W}_{ele} = \eta F_{pg} EA_{frontal} = 0.15 \cdot 0.8 \cdot 1360 \cdot (\pi \cdot 0.25^2) = 32$ W all the time during the typical 90 minutes of a LEO period. If this electrical energy is to be consumed in 15 min, the rate must be $32 \cdot 90 / 15 = 194$ W.

The thermal balance takes the form:

$$C \frac{dT}{dt} = \dot{Q}_{ele,dis} + \dot{Q}_s - \dot{Q}_{out} = \dot{Q}_{ele,dis} + \alpha_{th} EA_{frontal} - \varepsilon A \sigma T^4$$

$$\rightarrow 30 \cdot 10^3 \frac{dT}{dt} = 194 f_{dis}(t) + 169 - 33 \cdot 10^{-9} T^4$$

with T in [K], where $f_{dis}(t)$ is a periodic step function equal to 0 except for a 15 min period during the orbit, $\dot{Q}_s = \alpha_{th} EA_{frontal} = (0.75 - 0.15 \cdot 0.8) \cdot 1370 \cdot \pi \cdot 0.25^2 = 169$ W is the thermal absorption of the solar panels ($\alpha_{th} = \alpha - \eta F_{pg}$), and $\dot{Q}_{out} = \varepsilon A \sigma T^4 = 0.75 \cdot 4 \cdot \pi \cdot 0.25^2 \cdot 5.67 \cdot 10^{-8} T^4 = 33 \cdot 10^{-9} T^4$ the satellite own emission. Notice that an initial temperature value is required to solve the energy balance in general, but the periodic solution (presented in Fig. E3, from a numerical simulation) does not depend on it. Notice that spacecraft temperature increases during electrical dissipation and decreases otherwise (when infrared emission surpasses solar input).

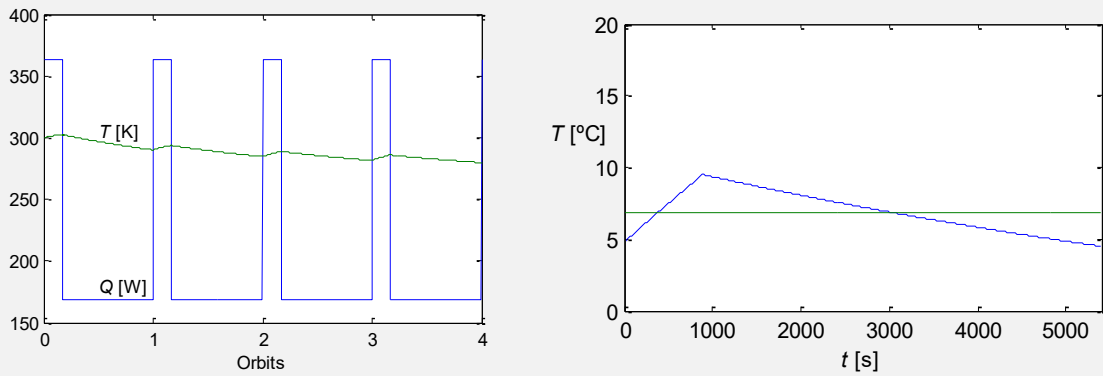


Fig. E3. Evolution of input loads ($\dot{Q}_{\text{ele,dis}} + \dot{Q}_s$) and satellite temperature (T) after an initial value of 300 K. Detail of the periodic temperature evolution and its orbit mean.

Effect of satellite geometry

We found above the steady temperature an isothermal body would attain when exposed only to the Sun (and the background radiation environment). What about a different geometry, like a cube box or a plate? The answer is similar:

$$0 = \alpha E A_{\text{frontal}} - \varepsilon A \sigma T^4 \rightarrow T = \left(\frac{A_{\text{frontal}}}{A} \frac{\alpha E}{\varepsilon \sigma} \right)^{\frac{1}{4}} \quad (12)$$

although now the area ratio is no longer $A_{\text{frontal}}/A=1/4$ as for a sphere.

Exercise 4. Find the steady temperature at 1 ua, for an isothermal blackbody with the following geometries: planar one-side surface (i.e. rear insulated), plate, cylinder, sphere, and cubic box in its three symmetric orientations.

Sol.: Steady energy balance for a body with frontal area A_f and emitting area A_e : $\alpha E A_f = \varepsilon A_e \sigma (T^4 - T_\infty^4)$, which, with $\alpha=1$ and $\varepsilon=1$, yields $T = [(A_f/A_e)(E/\sigma)]^{1/4}$.

For one-side planar surface of area A with its normal tilted an angle β to Sun rays, frontal area $A_f = A \cos \beta$, and emitting area $A_e = A$, thence $T = (\cos \beta E/\sigma)^{1/4}$, and for $\beta=0$, $T = [1360/(5.67 \cdot 10^{-8})]^{1/4} = 394 \text{ K} = 122 \text{ }^\circ\text{C}$.

For a plate emitting from both sides, $A_f = A \cos \beta$ and $A_e = 2A$, thence $T = ((\cos \beta/2)E/\sigma)^{1/4}$, and for $\beta=0$, $T = 332 \text{ K} = 59 \text{ }^\circ\text{C}$.

For a cylinder of diameter D and length L with its axis tilted an angle β to Sun rays, with all its surfaces emitting, $A_f = (\pi D^2/4) \cos \beta + (\pi D L \sin \beta)/2$ and $A_e = 2\pi D^2/4 + \pi D L$, thence $T = (((\cos \beta/2 + (L/D) \sin \beta)/(1 + 2L/D))E/\sigma)^{1/4}$, which, for $L/D=1$ and $\beta=0$ yields, $T = 252 \text{ K} = -21 \text{ }^\circ\text{C}$, and for $L/D=1$ and $\beta=\pi/2$ yields, $T = 300 \text{ K} = 26 \text{ }^\circ\text{C}$.

For a sphere, $A_f = \pi D^2/4$ and $A_e = \pi D^2$, thence $T = ((1/4)E/\sigma)^{1/4}$, and $T = 279 \text{ K} = 6 \text{ }^\circ\text{C}$.

For a frontal cube, i.e. an hexahedron of face area A , with all its surfaces emitting, $A_f = A$ and $A_e = 6A$, thence $T = ((1/6)E/\sigma)^{1/4}$, and $T = 252 \text{ K} = -21 \text{ }^\circ\text{C}$.

For a cube tilted 45° , i.e. an hexahedron with two opposite edges and the Sun in the same plane, $A_f = \sqrt{2}A$ and $A_e = 6A$, thence $T = ((\sqrt{2}/6)E/\sigma)^{1/4}$, and $T = 275 \text{ K} = 2 \text{ }^\circ\text{C}$.

For a cube pointing to the Sun, i.e. an hexahedron with two opposite vertices and the Sun in the same straight line (3 lit faces tilted 54.7° , instead of 2 lit faces tilted 45° in the previous case), $A_f = \sqrt{3}A$ and $A_e=6A$, thence $T=((\text{sqrt}(3)/6)E/\sigma)^{1/4}$, and $T=289\text{ K}=16^\circ\text{C}$.

Notice that only fully-convex surfaces have been considered; otherwise, view factors would enter into play. For instance, consider a hemispherical shell with its symmetry axis aligned with the Sun (it does not matter if it is the convex or the concave side facing the Sun), the energy balance is now:

$$0 = \alpha E A_{\text{frontal}} - \varepsilon (A_1 F_{1,\infty} + A_2 F_{2,\infty}) \sigma T^4 \rightarrow T = \left(\frac{\pi R^2}{2\pi R^2 (F_{1,\infty} + F_{2,\infty})} \frac{\alpha E}{\varepsilon \sigma} \right)^{\frac{1}{4}} = \left(\frac{\alpha E}{3\varepsilon \sigma} \right)^{\frac{1}{4}}$$

where $F_{1,\infty}=1$ and $F_{2,\infty}=1/2$ ([View factor tables](#)), resulting in $T=300\text{ K}=27^\circ\text{C}$. Notice that a hollow hemisphere gets warmer than a spherical shell, having the same frontal area and exposed area (27°C instead of 6°C), because the concave part re-radiates to itself.

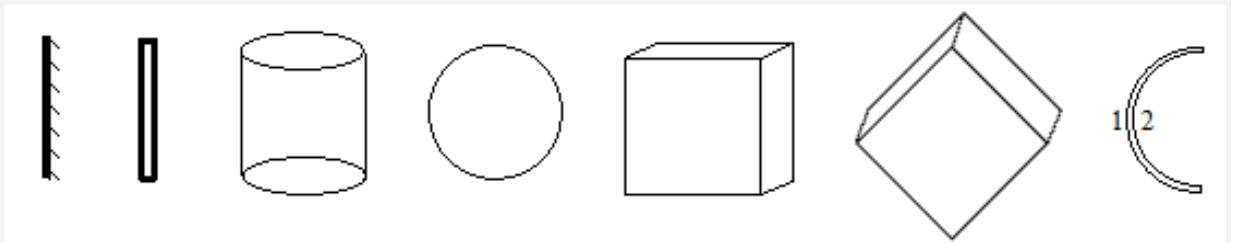


Fig. E4. Different geometries analysed.

Effect of a sunshield

Everybody knows that the best way to protect from sunshine is a sunshield. The simplest example to model may be an infinite planar shield in between two infinite parallel planar plates at fix temperatures T_1 and $T_2 < T_1$, all surfaces assumed to be black bodies. Without the shield, the heat transfer is $\dot{Q}_{12} = \sigma (T_1^4 - T_2^4)$, whereas in the case of the shield, when it gets at steady state at temperature T_i , its steady energy balance is $0 = \dot{Q}_{1,i} + \dot{Q}_{2,i} = \sigma (T_1^4 - T_i^4) + \sigma (T_2^4 - T_i^4)$, and thus $T_i = \left[\frac{(T_1^4 + T_2^4)}{2} \right]^{1/4}$ and $\dot{Q}_{1,i} = \dot{Q}_{i,2} = \dot{Q}_{1,2} / 2$, i.e. the heat transfer between the original surfaces has been halved.

Notice that we have assumed fix temperatures in the above example; if not, details of the energy balance at each end plate would have influenced the problem. Also notice that, contrary to the result of the above example, the effect of geometry is important in most cases (even in the one-dimensional problem with cylindrical or spherical geometries, the radial position of a shield dominates the problem, as shown [aside](#)).

Effect of a concavity

If we compare the thermal balance of a spherical shell of radius R with that of a hemispherical shell of the same radius and pointing to the Sun, both objects considered isothermal black bodies subjected only to solar radiation in space, we soon realise that the hemisphere gets warmer because both get the same solar input (i.e. for a solar irradiance E , both, sphere and hemisphere, get $E\pi R^2$). However, the sphere freely emits $\sigma 4\pi R^2 (T^4 - T_\infty^4)$, which we may ascribe to its two convex hemispheres, whereas the hemisphere, which has two hemispherical surfaces emitting, the external one (exposed to the Sun and empty space) and the internal one (which not only sees the empty space but its own surface). We call surface 1 the sunlit

hemisphere, and surface 2 the hemisphere in shadow, the heat transfer from 2 to background space is $\dot{Q}_{2,\infty} = \pi R^2 F_{2,\infty} \sigma (T_2^4 - T_\infty^4)$, with $F_{2,\infty} < 1$ easily obtained from the reciprocity relation $A_2 F_{2,3} = A_3 F_{3,2}$ (see [View factor algebra](#)), where surface 3 is the auxiliary circle surface that would close the hemisphere to form a radiation closure and thus with $F_{3,2} = 1$. Thence, $F_{2,\infty} = F_{2,3} = A_3 F_{3,2} / A_2 = \pi R^2 \cdot 1 / (2\pi R^2) = 1/2$, as in Exercise 4, above.

Effect of planet: eclipse and own emission

When in addition to our system (a spacecraft or a part of it) and the Sun, the presence of a third body is considered (a celestial body like a planet or moon, or an artificial object), several effects on the thermal balance of the former may take place:

- Blocking the Sun, if the third body is in between, eclipsing our system from solar radiation sunshine (as the sunshield considered above), with the consequent cooling and loss of solar-panel power.
- Reflecting sunshine (albedo), if the third body is on one side, what adds a heat source (and solar-panel power, if any). This contribution is difficult to model because of the interplay of geometrical and thermo-optical variables, and the analysis is usually restricted to low altitude orbits, where albedo exitance is almost uniform in the whole field of view (e.g. from the 400 km of ISS altitude, only a surface patch 2300 km in diameter is seen).
- Besides, at any position, the third body radiates in the infrared due to its own temperature, what is an additional heat input to our system (both during daytime and night-time).

From those three effects, the most important is the eclipse, because it blocks the radiation from the Sun (a blackbody at 5800 K with good approximation), leaving instead the radiation from the planet, which may be approximated to a blackbody at a much lower temperature (between 100 K and 700 K in all cases).

We only consider total eclipse (umbra region), since partial eclipse (penumbra region) is only important when the planet or moon is far from the spacecraft, or for very special orbits at low altitudes.

Eclipse duration. Orbital solar angle

Eclipse duration is studied aside in [Orbital period and eclipse fraction](#), with the main result that, for circular orbits, the relative eclipse period, T_e/T_o (eclipse duration divided by orbital period), as a function of relative orbit radius, $h \equiv (H+R)/R$, and of beta angle, β (angle between the orbital plane and the solar direction, negative for retrograde orbits, i.e. $-\pi/2 \leq \beta \leq \pi/2$) is given by:

$$\frac{T_e}{T_o} = \frac{1}{\pi} \arccos \left(\frac{\sqrt{h^2 - 1}}{h \cos \beta} \right), \text{ with } \beta < \beta_{\max} = \frac{\pi}{2} - \arccos \frac{1}{h}, \text{ and } T_o = 2\pi \sqrt{\frac{(H+R)^3}{GM}} \quad (13)$$

where $G = 6.67 \cdot 10^{-11} \text{ N} \cdot \text{m}^2 / \text{kg}^2$ is the universal gravitation constant, M is the mass of the planet (can be obtained from [Planet and moon property tabulations](#)), and the beta angle is $\beta = 0$ for any orbit passing through the subsolar point (i.e. when the Sun is in the orbit plane, which may happen at any orbital inclination, $0 \leq i \leq \pi$), and $\beta = \pi/2$ when the orbital plane is perpendicular to Sun rays (i.e. when the satellite nadir follows the planet terminator, as for a polar orbit initiated at local dawn or dusk on an equinox).

If the angular position of the object along the circular orbit, ϕ , is measured starting from the direction nearer the Sun direction, the angles when eclipse starts, ϕ_{es} , and eclipse ends, ϕ_{ee} , are:

$$\left. \begin{aligned} \phi_{es} &= \pi - \arccos\left(\frac{\sqrt{h^2 - 1}}{h \cos \beta}\right) \xrightarrow{\beta=0} \pi - \arcsin \frac{1}{h} \\ \phi_{ee} &= \pi + \arccos\left(\frac{\sqrt{h^2 - 1}}{h \cos \beta}\right) \xrightarrow{\beta=0} \pi + \arcsin \frac{1}{h} \end{aligned} \right\} \quad (14)$$

For instance, for a $H=400$ km orbit like that of the ISS, $h=(H+R)/R=1.063$, maximum beta angle for eclipses to occur is $\beta_{max}=\pi/2-\arccos(1/h)=1.22=70.2^\circ$, therefore, any satellite at that altitude with an orbital inclination $i>\beta_{max}-\delta_{max}=70.2-23.5=46.7^\circ$ may potentially be sunlit during the whole orbit (the ISS has $i=52^\circ$ so that there are periods along the year without eclipse). For maximum eclipse duration ($\beta=0$), eclipse starts at $\phi_{es}=\pi-\arccos(\sqrt{1-1/h^2})=1.92=110^\circ$, and ends at $\phi_{ee}=2\pi-\phi_{es}=4.4=250^\circ$.

It is recommended to only use positive ϕ -angles (as done in (14), i.e. $\phi_{ee}=2\pi-\phi_{es}$, instead of $\phi_{ee}=-\phi_{es}$), if variable ϕ is to be used as a more convenient time variable, $\phi=t(2\pi/T_o)$. Notice that solar input to orbiting spacecraft with eclipse period has a discontinuity at eclipse-start and eclipse-end (we neglect the fraction of time in penumbra), and should be programmed accordingly, i.e. direct solar input, $\dot{Q}_s = \alpha A_{\text{frontal}} E$, becomes:

$$\dot{W}_{\text{em,in,solar}} = \dot{Q}_s = \dot{Q}_{s0} F_e = \alpha_b A_{\text{frontal}} E_s F_e, \quad \text{with} \quad F_e = \begin{cases} 0 & \text{if } \phi_{es} < \phi < \phi_{ee} \\ 1 & \text{otherwise} \end{cases} \quad (15)$$

where the symbol $\dot{W}_{\text{em,in,solar}}$ has been used to point out that this energy input is not properly a heat exchange (it is an electromagnetic input that might be nearly fully converted to work), but the symbol \dot{Q}_s (solar heat input) is commonly used. In (15) α_b and A_{frontal} are the body-surface solar-absorptance and the frontal area (recall that α_b should be substituted by $\alpha_{b,\text{th}}$ for solar cells, as explained above), E_s is the direct irradiance from the Sun, and F_e is the solar-eclipse ‘view function’: 1 if sunlit, 0 if in eclipse. Notice that eclipse duration cannot be large except for very high orbits, of little practical interest except in the case of satellites orbiting a planet moon, in which case the moon eclipse by the planet may add to the eclipse by the moon. For instance, low Earth orbit eclipse cannot last more than 40 minutes, and geostationary eclipses no more than 70 minutes, but for a spacecraft orbiting the Moon, more than 200 minutes of eclipse of the Moon by the Earth may add to the 45 minutes of lunar eclipse.

The eclipse period is usually the worst case for thermal control, and some heating is usually required to avoid the temperatures of sensitive instruments falling below their operational margins at the end of eclipse. High temperature gradients at the beginning and end of the eclipse period can be dangerous too, because of thermal expansion problems.

Planet own emission

Planets and moons emit thermal radiation proportional to the fourth power of its absolute temperature, invisible to our eyes because at moderate temperatures (maximum surface temperature in a solar planet is 735 K at Venus) practically all emitted radiation lies in the far infrared (i.e. $\lambda > 1 \mu\text{m}$). This planet-emission is an additional energy input to orbiting spacecraft, which can be either accounted solely as a ‘heat’ input by absorption of planet exitance, $\dot{Q}_{p,\text{in}} = \varepsilon_b A_b F_{b,p} M_p$ (recall that body absorptance in the far-infrared band equals emissivity, ε_b), or as (net) heat transfer, $\dot{Q}_{p,b} = \varepsilon_b A_b F_{b,p} M_p - A_b F_{b,p} M_b$, in terms of planet and spacecraft exitances in the far infrared, $M_p = \varepsilon_p \sigma T_p^4$ and $M_b = \varepsilon_b \sigma T_b^4$. The common practice in spacecraft thermal control is to take planet IR solely as an input ($\dot{Q}_{p,\text{in}}$), and include the spacecraft IR output to the planet in the output-to-background term, which is modelled also as a IR output and not as a heat exchange, in view of the low background temperature ($T_\infty = 2.7 \text{ K}$): $\dot{Q}_{\text{out}} = \varepsilon_b A_b \sigma T_b^4$. Hence, with the assumption of uniform planet temperature, planet IR input (usually called simply planet input, since the other planet contribution, albedo, is always treated apart), is constant along a circular orbit, and amounts to:

$$\dot{Q}_{p,\text{in}} = \varepsilon_b A_b F_{b,p} \varepsilon_p \sigma T_p^4 \quad (16)$$

where ε_b and A_b are the body surface absorptance in the infrared (equal to emissivity) and body area, $F_{b,p}$ is the view factor from body surface to planet surface (to be found in [View factor tabulations](#)), and ε_p and T_p are planet emissivity and surface temperature (to be found on [Planets and moons property tabulations](#)). Notice that the IR irradiance at an orbit altitude H , from an isothermal planet, decreases as the square of the radius, $E(H) = \varepsilon \sigma T_p^4 (R_p / (R_p + H))^2$. Notice that photovoltaic cells cannot convert IR radiation to electricity and thus planet input only has a heating effect.

Effect of planet: albedo

When not under eclipse, a satellite is always exposed to the reflected sunrays from the planet or moon (its albedo or ‘whiteness’), and maybe from nearby spacecraft parts. The maximum albedo contribution for a given spacecraft altitude would take place at the subsolar point (for orbits passing by) on a nadir-facing surface (Fig. 2a); other more intricate layouts as shown in Fig. 2b are treated afterwards.

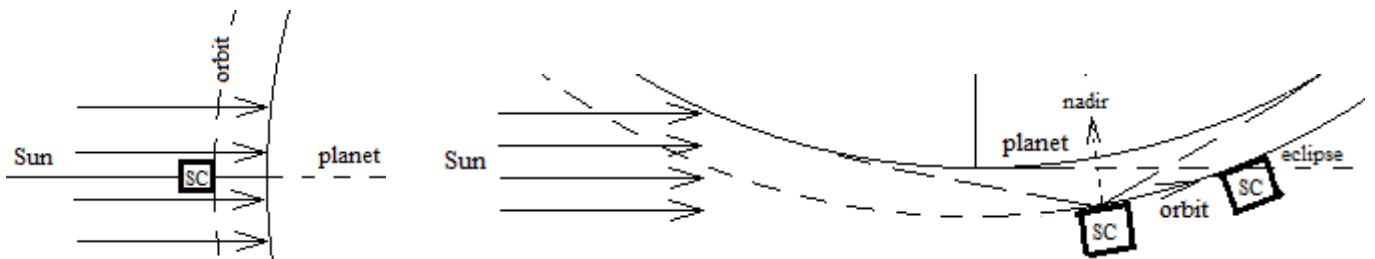


Fig. 2. Extreme cases in albedo contribution to low-orbiting spacecraft (SC): a) SC at subsolar point, b) SC near entering eclipse.

First consider a cube-box satellite facing nadir in low orbit (say with altitude over planet radius $H/R < 0.1$; $H < 600 \text{ km}$ for LEO), at the subsolar point (Fig. 2a). Solar reflection at the planet surface is $\rho_p E_s$, where ρ_p is the planet reflectance to solar radiation (albedo), and E_s is the solar irradiance at subsolar point ($E_s = 1360 \text{ W/m}^2$). In the limit of very low orbits, the reflected irradiance falling on the satellite nadir surface will be

the same because it approaches a planar one-dimensional geometry (for Earth, with $\rho_p=0.3$, this albedo irradiance on a planar surface facing the subsolar point is $E_a=\rho_p E_s=0.3 \cdot 1360=410 \text{ W/m}^2$; the radiation absorbed by the nadir surface is $\alpha_b A_b \rho_p E_s$, where α_b is the absorptance of the body-surface considered (in the solar band, to be found on [Planets and moons property tabulations](#), but notice that for solar panels with photovoltaic cells of energy efficiency η covering an area fraction F_{pq} , the thermal absorptance is only $\alpha_b - \eta F_{pq}$), and A_b its area. For finite altitudes we must introduce the view factor, i.e. the fraction of frontal semi-space occupied by the planet (or fraction of radiation emitted by A_b that will impinge on the planet), $F_{b,p}$, which can be found in [View factor tabulations](#) and is $F_{b,p}=(R_p/(R_p+H))^2$. The reflected solar energy absorbed by the nadir surface is thus:

$$\dot{W}_{em,in,alb,max} = \dot{Q}_{a0} = \alpha_b A_b F_{b,p} \rho_p E_s \quad (17)$$

where the symbol $\dot{W}_{em,in,alb,max}$ has been used to point out that this energy input is not properly a heat exchange (it is an electromagnetic input that might be nearly fully converted to work), but the symbol \dot{Q}_{a0} ('heat input' from albedo at subsolar angle $\phi=0$) is commonly used. It is worth plotting the variation of albedo irradiance with orbit altitude, as shown in Fig. 3, where it is compared with the irradiance on the same nadir-facing surface due to planet own emission, (16)).

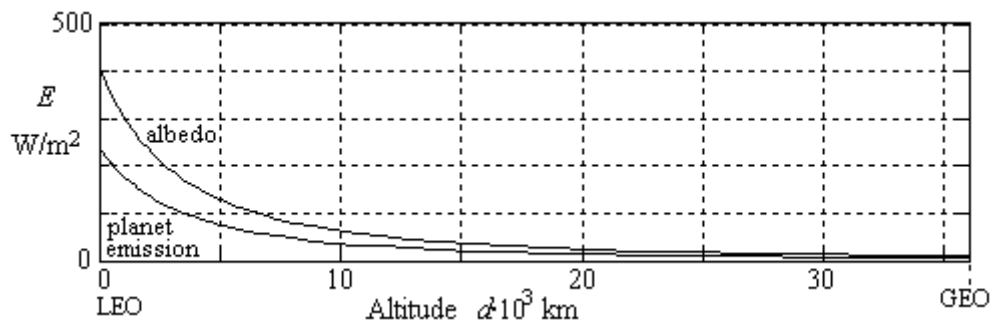


Fig. 3. Albedo irradiance (and planet IR emission emittance) on a planar surface facing the subsolar point, as a function of altitude for Earth orbits.

We may deduce several general conclusions from Figs. 2 & 3:

- Maximum albedo irradiance, and planet IR irradiance, quickly decrease with altitude, H , and their contribution to the energy balance of spacecraft parts is often negligible except for low orbits (say $h \equiv H/R < 3$); e.g. the 410 W/m^2 albedo irradiance at $H \rightarrow 0$ drops to $E_a = \rho_p E_s F_{b,p} = 0.3 \cdot 1360 \cdot 0.06 = 24 \text{ W/m}^2$ for a mid-altitude Earth orbit of $H=20\,000 \text{ km}$ as used for navigation satellites.
- Albedo irradiance at high orbits is really smaller than as given by (17) because, contrary to own emission from a diffuse sphere (e.g. a blackbody), the reflected radiation from the incident collimated solar beam is not seen as a uniform bright but decays to zero at the planet limb (if the planet is assumed perfectly diffusive; in practice, most real objects, and planets and moons in particular, show different degrees of retro-reflecting effect, as shown in Fig. 4).
- Contrary to what Fig. 3 might suggest, albedo input is usually smaller than planet-IR input on spacecraft thermal control, because the former rapidly decreases out of the subsolar position (it is zero during eclipse, see Fig. 2), while the latter remains practically the same all along the orbit.

Besides, those maximum values are lowered by the respective absorptance of the surface involved (for albedo, in the solar band, α ; for the planet emission, in the IR band, ε).

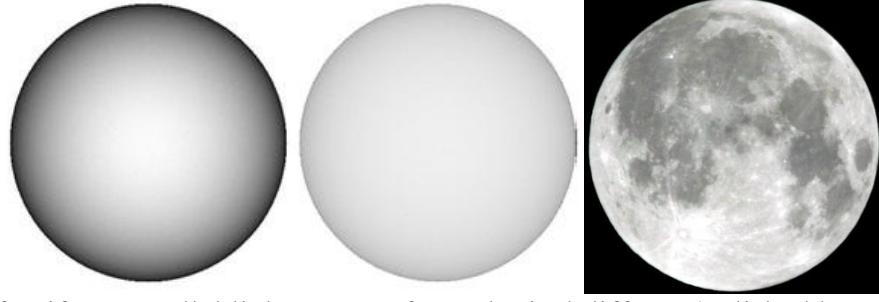


Fig. 4. a) Reflection of uniform parallel light on a perfect spherical diffuser (polished but Lambertian, not specular). b) Reflection on a real rough-surface sphere (with some retro-reflection at the rim). Not to be confused with own emission from an isothermal sphere, which would be seen (with a thermal camera for $T < 1000$ K) nearly uniformly bright if Lambertian. c) Full moon reflectance (deep retro-reflection).

Properly computing the albedo view factor at any point in the orbit (i.e. for a non-zero phase angle) is a very hard task because of the bidirectional dependence (Sun direction and viewing direction) and the conical perspective (satellite close to the planet). That difficulty, together with the non-Lambertian behaviour of real surfaces, and the rapid changes in the field of view from the spacecraft, makes a simpler albedo model more convenient.

For low orbits (say for altitudes less than 5% of planet radius, i.e. < 320 km LEO), the flat-planet model may be good because only 2000 km of Earth's surface is under the field of view, and that patch may be assumed uniformly illuminated by the Sun. If the patch centre, the Earth's centre, and the Sun, form an angle θ , the patch will get a solar irradiance $E_0 \cos \theta$. Using the spherical law of cosines, $\cos \theta = \cos \phi \cos \beta$, where ϕ is the spacecraft angular position in its orbit, and β the orbit solar angle, as defined above; for an orbit passing by the sub-solar point, $\beta = 0$ and consequently $\theta = \phi$. The absorbed albedo radiation can be set as:

$$\dot{Q}_a = \dot{Q}_{a0} F_a, \quad F_a = \cos \phi \cos \beta F_e, \quad F_e = \begin{cases} 1 & \text{if } -\pi/2 < \phi < \pi/2 \\ 0 & \text{otherwise} \end{cases} \quad (18)$$

where \dot{Q}_{a0} is the absorbed albedo radiation corresponding to the subsolar point, given by (17), whether the satellite passes through that point or not.

For high orbits, computing albedo input is more difficult because the satellite may see a wider surface area on the planet, differently illuminated by the Sun. The limit case would be for very high orbits ($H \rightarrow \infty$), from which the lit part of the planet would be seen as a lune or crescent, i.e. the area between the planet limb and the terminator (the line separating the illuminated and dark parts, which is half an ellipse in orthogonal projection). If θ is the phase angle (like for Moon phases seen from Earth, i.e. the angle between the planet-to-Sun and planet-to-observer lines), it is easy to compute the crescent area as seen from afar, $A_{\text{crescent}} = \pi R^2 (1 + \cos \theta) / 2$. Notice that from such a far distance the eclipse orbit fraction tends to zero (only

when the satellite and Sun are in opposition there is no albedo). But albedo input tends to zero at such high distances due to the view factor F_{bp} in (17) and are of no concern to thermal control. Albedo input at intermediate orbit-altitudes, i.e. not in the limit $H \rightarrow 0$, can be estimated with the empirical fitting:

$$\dot{Q}_a = \dot{Q}_{a0} F_a, \quad F_a = \left(\frac{1 + \cos \phi}{2} \right)^2 \left[1 - \left(\frac{\phi}{\phi_{es}} \right)^2 \right] \cos \beta F_e, \quad F_e = \begin{cases} 1 & \text{if } -\phi_{es} < \phi < \phi_{es} \\ 0 & \text{otherwise} \end{cases} \quad (19)$$

in substitution of (18), where, as above, the absorbed albedo radiation corresponding to the subsolar point, \dot{Q}_{a0} is $\dot{Q}_{a0} = \alpha_b A_b F_{b,p} \rho_p E_s$ (or $\dot{Q}_{a,th,0} = (\alpha_b - \eta F_{pq}) A_b F_{b,p} \rho_p E_s$ for photovoltaic generators). Notice that (19) is only valid for satellite orbits with eclipse periods (i.e. for $T_e > 0$ in (13), which sets the limit in β), when ϕ_{es} is well defined. Notice also that the restriction on maximum solar orbit-solar-angle, β , given by (13) applies to both (18) and (19) models, which are compared in Fig. 5. In any case, the ϕ -bounds on (18) and (19) only apply to the first orbit, $-\pi < \phi < \pi$, to extend the computations to subsequent orbits, a floating-point remainder (modulo operation) must be used, i.e. ϕ must be substituted by $\phi - 2\pi \text{ floor}((\phi + \pi)/(2\pi))$.

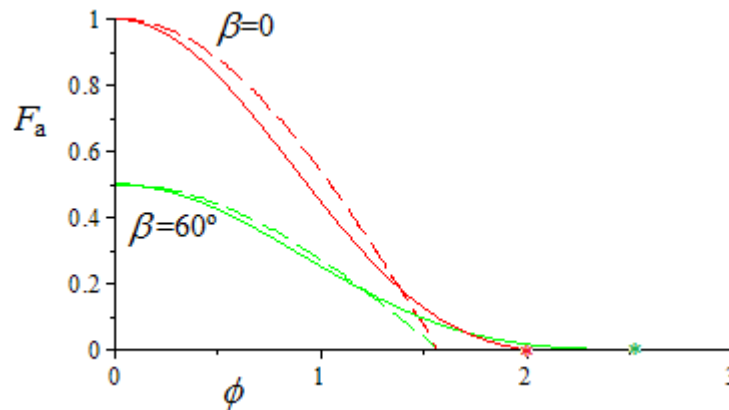


Fig. 5. Albedo factor F_a function versus orbit angle ϕ , for a low orbit with $h \equiv H/R = 0.1$ relative altitude. Comparison between the simple cosine model (18) and the extended model (19) for two orbit-solar-angle values: $\beta = 0$ (the orbit cuts through the sub-solar direction, and eclipse starts at $\phi_{es} = 2.0$ rad), and $\beta = 60^\circ = 1.05$ rad (eclipse starts at $\phi_{es} = 2.6$ rad).

Exercise 5. Consider a spherical black-body of 1 m in diameter, in an equatorial orbit at 300 km Earth altitude. Find:

- Orbital period and eclipse duration.
- Solar input along the orbit.
- Infrared input from the planet, assumed at a temperature of 288 K and with $\varepsilon = 0.6$.
- Albedo input along the orbit, assuming an albedo of 0.3 and a simple albedo model.
- Periodic temperature evolution, assuming the body is isothermal, with a mass of 50 kg and a thermal capacity of 1000 J/(kg·K).

Sol.:

- Orbital period and eclipse duration.

An Equatorial orbit is in the Equatorial plane, which, for the Earth, is tilted 23.5° to the ecliptic plane. The subsolar point (i.e. the intersection of the Sun-planet direction with the sphere of the planet) is only at the Equator on equinoxes (20 March and 22 September), and then the eclipse last

the longest (although the seasonal variation is small for Equatorial orbits; the minimum eclipse time is at solstices, with $T_e=35.5$ min instead of 36.5 min). For $H=300$ km and Earth radius $R=6370$ km, $h=(H+R)/R=1.047$, and from orbit mechanics (13) with $G=6.67310^{-11}$ N·m²/kg² and Earth mass $M=5.97 \cdot 10^{24}$ kg, we get the orbit period, $T_o=5420$ s (90 min), and from (14) the eclipse duration $T_e=2190$ s (36.5 min), eclipse start angle $\phi_{es}=1.87$ rad (107°), and eclipse end angle $\phi_{ee}=4.41$ rad (253°); see Fig. E5.1

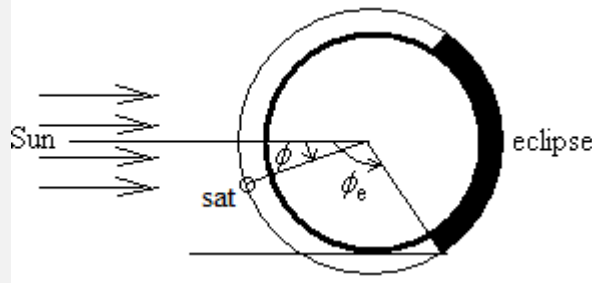


Fig. E5.1. Eclipse zone (in black) for a spherical satellite in a low Earth orbit passing through the subsolar point $\phi=0$.

b) Solar input along the orbit.

The energy absorbed (or 'heat input') is constant on the sunlit sphere, and zero during eclipse. We must set up a step function to signal eclipses, but, in order for it to be valid for angles beyond 2π (which are needed for multi-orbit simulation), we need a function to wrap up any orbit angle to the $0..2\pi$ interval, which is accomplished with the function $f(\phi)=\phi \bmod 2\pi$ (i.e. the fractional part in the division $\phi/(2\pi)$; see Fig. E5.2).

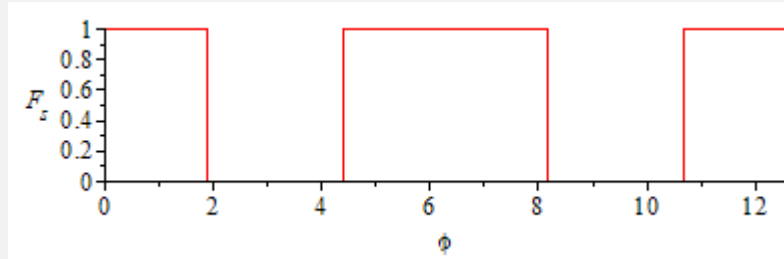


Fig. E5.2. Eclipse function F_e (1 if sunlit, 0 if in eclipse) for two consecutive orbits (ϕ in [rad]).

Solar input (15) is then programmed as:

$$\dot{Q}_s = \dot{Q}_{s0} F_e = \alpha_b A_{\text{frontal}} E_s F_e, \quad \text{with} \quad F_e = \begin{cases} 0 & \text{if } \phi_{es} < (\phi \bmod 2\pi) < \phi_{ee} \\ 1 & \text{otherwise} \end{cases}$$

with $\dot{Q}_{s0} = \alpha_b A_{\text{frontal}} E_s = 1 \cdot (\pi D^2/4) E_s = 1 \cdot (\pi \cdot 1^2/4) \cdot 1360 = 1076$ W; i.e. the 1 m in diameter spherical blackbody gets 1076 W directly from the Sun when lit, zero otherwise.

c) Infrared input from the planet, assumed at a temperature of 288 K and with $\varepsilon=0.6$.

If the planet is assumed isothermal, the infrared input is constant along the orbit, $\dot{Q}_{p,\text{in}} = \varepsilon_b A_b F_{b,p} \varepsilon_p \sigma T_p^4$ (notice that the infrared emissivity of the object surface is used instead

of its absorptance in the IR, since they are equal). The view factor from body to planet, $F_{b,p}$ (i.e. from a small sphere to a much larger sphere) is found in View factor tabulations to be:

$$F_{b,p} = \frac{1 - \sqrt{1 - \frac{1}{h^2}}}{2} = 0.35$$

and thus $\dot{Q}_{p,in} = \varepsilon_b A_b F_{b,p} \varepsilon_p \sigma T_p^4 = 1 \cdot (\pi 1^2) \cdot 0.35 \cdot 0.6 \cdot (5.67 \cdot 10^{-8}) \cdot 288^4 = 259 \text{ W}$.

d) Albedo input along the orbit, assuming an albedo of 0.3 and a simple albedo model.

Maximum albedo input occurs at subsolar position and is (with albedo $\rho_p=0.3$):

$$\dot{Q}_{a0} = \alpha_b A_b F_{b,p} \rho_p E_s = 1 \cdot (\pi 1^2) \cdot 0.35 \cdot 0.3 \cdot 1360 = 454 \text{ W}$$

Albedo input at any point along the orbit is:

$$\dot{Q}_a = \dot{Q}_{a0} F_a, \quad F_a = \left(\frac{1 + \cos \phi}{2} \right)^2 \left[1 - \left(\frac{\phi}{\phi_{es}} \right)^2 \right] F_c, \quad F_c = \begin{cases} 0 & \text{if } -\phi_{es} < \phi < \phi_{es} \\ 1 & \text{otherwise} \end{cases}$$

The albedo factor, F_a , has been plotted in Fig. E5.3 for two consecutive orbits.

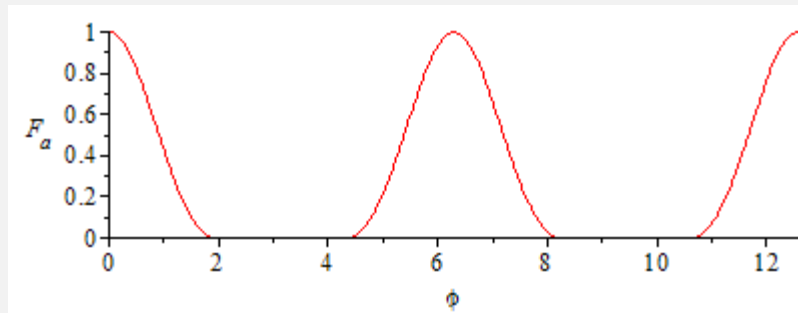


Fig. E5.3. Albedo function F_a (1 at the subsolar point, 0 if in eclipse) for two consecutive orbits (ϕ in [rad]).

e) Periodic temperature evolution, assuming the body is isothermal, with a mass of 50 kg and a thermal capacity of 1000 J/(kg·K).

The energy balance is $dE/dt = \dot{W} + \dot{Q} = 0 + \dot{Q}_s + \dot{Q}_a + \dot{Q}_p - \dot{Q}_\infty$, since there is no mechanical or electrical work, there are three inputs (solar, albedo, and planet), and one output (to the background environment). Substitution of $dE=mc dT$ and previous results yields:

$$mc \frac{dT}{dt} = \dot{Q}_{s0} F_c(\phi) + \dot{Q}_{a0} F_a(\phi) + \dot{Q}_p - \dot{Q}_\infty = \\ = \alpha_b A_{\text{frontal}} E_s F_c(\phi) + \alpha_b A_b F_{b,p} \rho_p E_s F_a(\phi) + \varepsilon_b A_b F_{b,p} \varepsilon_p \sigma T_p^4 - \varepsilon_b A_b F_{b,\infty} \sigma T^4$$

where the last term, the own emission from the body of emissivity ϵ_b , has a view factor of unity, $F_{b,\infty}=1$, because the spherical surface is fully convex and only sees ‘background space’ (recall that only inputs from the Sun and the planet were accounted for, not net exchange).

The above energy balance is a first-order ordinary differential equation in $T(t)$ (or $T(\phi)$, since $t/T_o=\phi/(2\pi)$), which must be solved with some initial conditions (e.g. $T(0)=300$ K) until transients decay and a periodic solution remains. This can be done by Euler's method or better by some Runge-Kutta method. A numerical simulation with time discretization $\Delta t=100$ s has been run for $N=5$ orbits (until $t_{\text{end}}=NT_o=5\cdot 5424=27120$ s, starting with $T(0)=300$ K, and is presented in Fig. E5.4.

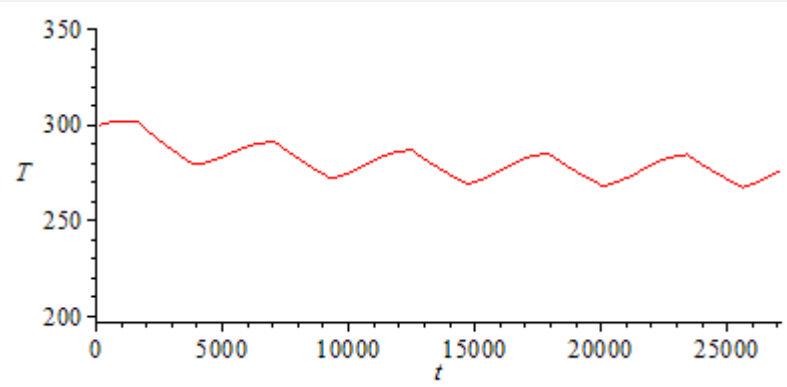


Fig. E5.4. Temperature evolution of the isothermal sphere with time for 5 consecutive orbits (with T in [K] and t in [s]), from an arbitrary initial state at the subsolar point $T(0)=300$ K.

We see in Fig. E5.4 that the 5th orbit (five have been simulated) is already periodic (notice that the initial and final T -values must coincide to be periodic), and we plot it alone in detail in Fig. E5.5 (minimum, mean, and maximum values are 268 K, 276 K, and 285 K).

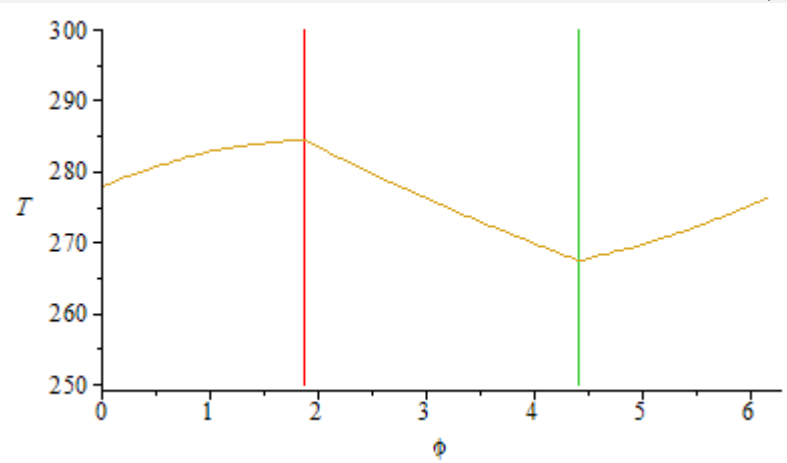


Fig. E5.5. Temperature evolution in the periodic state (the 5th orbit in Fig. E5.4 is plot, but in orbit angle units (T in [K] and ϕ in [rad])),

Notice in Fig. E5.5 the abrupt change in the slope of $T(t)$ at entry and exit of eclipse, $\phi_{\text{es}}=1.87$ rad and $\phi_{\text{ee}}=4.41$ rad.

A combination of albedo from Earth and from another body can be found in a [solved exercise](#) aside (in Spanish) where the external thermal loads on a balloon's gondola are computed.

Analytical one-node sinusoidal solution

The basic goal of thermal analysis is finding the spatial temperature distribution (always discretized to a number of isothermal parts, the nodes; for the time being a single node, i.e. an isothermal body), and the temporal temperature evolution. This goal is achieved by solving the energy balance equation:

$$mc \frac{dT}{dt} = \dot{Q}_{s0} F_c(\phi) + \dot{Q}_{a0} F_a(\phi) + \dot{Q}_p - \dot{Q}_\infty = \alpha_b A_{\text{frontal}} E_s F_c(\phi) + \alpha_b A_b F_{b,p} \rho_p E_s F_a(\phi) + \varepsilon_b A_b F_{b,p} \varepsilon_p \sigma T_p^4 - \varepsilon_b A_b F_{b,\infty} \sigma T^4 \quad (20)$$

what has to be done numerically because of the non-linear terms in the energy inputs (the eclipse factor F_c , and the albedo factor F_a ; except in the special case of Sun-synchronous orbits), and the non-linear term in the energy output (T^4). But we have seen in previous examples that, for low altitude orbits, the input loads follow an up-and-down pattern: high gains when under sunshine, low gains under eclipse (just by planet emission), so that a cosine modulation over the average may be a suitable first approximation, i.e. we set $F_c=F_a=(1+\cos\phi)/2$. We have seen too, that temperature variations are not so great (a few tens of kelvin around 300 K or so), what suggest that Eq. (20) may be linearized in the temperature excursion, i.e. we set $T(t)=T_m+\Delta T(t)$, which, after some transients, must develop a periodic solution that in the linear case is just a retarded cosine function (due to thermal inertia), i.e. in orbit angles (recall that $t/T_o=\phi/(2\pi)$):

$$T(\phi)=T_m+T_a\cos(\phi-\varphi) \quad (21)$$

where the mean temperature value, T_m , the amplitude of the temperature oscillation, T_a , and the phase lag, φ , are obtained by substituting in Eq. (20), linearizing the T^4 -term, expanding the combined trigonometric functions, and cancelling the coefficients in $\cos\phi$, in $\sin\phi$, and the independent terms, i.e.:

$$mc \frac{2\pi}{T_o} [-T_a \sin(\phi-\varphi)] = \alpha_b A_{\text{frontal}} E_s \frac{1+\cos(\phi)}{2} + \alpha_b A_b F_{b,p} \rho_p E_s \frac{1+\cos(\phi)}{2} + \varepsilon_b A_b F_{b,p} \varepsilon_p \sigma T_p^4 - \varepsilon_b A_b F_{b,\infty} \sigma [T_m^4 + 4T_m^3 T_a \cos(\phi-\varphi)] \quad (22)$$

with the independent terms yielding the mean temperature, T_m :

$$0 = \frac{\alpha_b A_{\text{frontal}} E_s}{2} + \frac{\alpha_b A_b F_{b,p} \rho_p E_s}{2} + \varepsilon_b A_b F_{b,p} \varepsilon_p \sigma T_p^4 - \varepsilon_b A_b F_{b,\infty} \sigma T_m^4 \Rightarrow T_m = \left[\frac{F_{b,p} \varepsilon_p}{F_{b,\infty}} T_p^4 + \frac{\alpha_b A_{\text{frontal}} E_s + \alpha_b A_b F_{b,p} \rho_p E_s}{2\varepsilon_b A_b F_{b,\infty} \sigma} \right]^{\frac{1}{4}} \quad (23)$$

the $\sin\phi$ -terms yielding the phase lag, φ (notice the mc -dependence):

$$-mc \frac{2\pi}{T_o} T_a \cos \varphi = -\varepsilon_b A_b F_{b,\infty} \sigma 4T_m^3 T_a \sin \varphi$$

$$\Rightarrow \varphi = \arctan \frac{\pi mc}{2\varepsilon_b A_b F_{b,\infty} \sigma T_m^3 T_o}$$
(24)

(mind that T_o is the orbit period), and the $\cos \varphi$ -terms yielding the temperature oscillation amplitude, T_a (proportional to solar and albedo fluctuations):

$$mc \frac{2\pi}{T_o} T_a \sin \varphi = \frac{\alpha_b A_{\text{frontal}} E_s}{2} + \frac{\alpha_b A_b F_{b,p} \rho_p E_s}{2} - \varepsilon_b A_b F_{b,\infty} \sigma 4T_m^3 T_a$$

$$\Rightarrow T_a = \frac{\alpha_b A_{\text{frontal}} E_s + \alpha_b A_b F_{b,p} \rho_p E_s}{2 \left(\frac{2\pi mc \sin \varphi}{T_o} + \varepsilon_b A_b F_{b,\infty} \sigma 4T_m^3 \right)}$$
(25)

Of course, one cannot expect very accurate predictions from this linear one-node approximation, but it is a very helpful guide during preliminary attempts to spacecraft thermal control, where body geometry, orbit details, surface finishing and so on, may be unknown.

Exercise 6. Consider a spherical black-body of 1 m in diameter, with a mass of 50 kg and a thermal capacity of 1000 J/(kg·K), in an equatorial orbit at 300 km Earth altitude. A linear one-node model is to be used for preliminary thermal analysis. Find:

- The linear mean temperature along an orbit, and its comparison with the non-linear average.
- The amplitude of the linear temperature oscillations.
- The angle and time lag of the temperature response (relative to the subsolar point).
- A plot of the predicted temperature evolution.

Sol.:

- a) The linear mean temperature along an orbit, and its comparison with the non-linear average.

This is a simplification of Exercise 5, from which we borrow without development the following results:

- Relative orbit radius, $h \equiv (H+R)/R = 1.047$.
- Orbit period, $T_o = 5429$ s.
- Eclipse duration, $T_e = 2190$ s.
- Eclipse start angle (from subsolar point), $\phi_{es} = 1.87$ rad.
- Eclipse end angle (from subsolar point), $\phi_{es} = 4.41$ rad.
- Solar input at subsolar point, $\dot{Q}_{s0} = \alpha_b A_{\text{frontal}} E_s = 1 \cdot (\pi D^2/4) E_s = 1 \cdot (\pi \cdot 1^2/4) \cdot 1360 = 1076$ W.
- Planet input (constant), $\dot{Q}_{p,\text{in}} = \varepsilon_b A_b F_{b,p} \rho_p \sigma T_p^4 = 1 \cdot (\pi 1^2) \cdot 0.35 \cdot 0.6 \cdot (5.67 \cdot 10^{-8}) \cdot 288^4 = 259$ W.
- Albedo input at subsolar point, $\dot{Q}_{a0} = \alpha_b A_b F_{b,p} \rho_p E_s = 1 \cdot (\pi 1^2) \cdot 0.35 \cdot 0.3 \cdot 1360 = 454$ W.
- Radiation emitted, $\dot{Q}_\infty = \varepsilon_b A_b F_{b,\infty} \sigma T^4 = 1 \cdot (\pi 1^2) \cdot 0.35 \cdot (5.67 \cdot 10^{-8}) \cdot T^4$ (with T in [K] and \dot{Q}_∞ in [W]).
- Energy balance:

$$\begin{aligned}
mc \frac{dT}{dt} &= \dot{Q}_{s0} F_c(\phi) + \dot{Q}_{a0} F_a(\phi) + \dot{Q}_p - \dot{Q}_\infty = \\
&= \alpha_b A_{\text{frontal}} E_s F_c(\phi) + \alpha_b A_b F_{b,p} \rho_p E_s F_a(\phi) + \varepsilon_b A_b F_{b,p} \varepsilon_p \sigma T_p^4 - \varepsilon_b A_b F_{b,\infty} \sigma T^4
\end{aligned}$$

Now the linearized solution is expected to be:

$$T(\phi) = T_m + T_a \cos(\phi - \varphi)$$

where the linearized mean temperature value, T_m , the amplitude of the temperature oscillation, T_a , and the phase lag, φ , are obtained by substituting $T(\phi) = T_m + T_a \cos(\phi - \varphi)$, $dT/dt = (2\pi/T_o) dT/d\phi$, $F_c(\phi) = (1 + \cos\phi)/2$, and $F_a(\phi) = (1 + \cos\phi)/2$, in the above energy balance, linearizing the T^4 -term, expanding the combined trigonometric functions, and cancelling the coefficients in $\cos\phi$, in $\sin\phi$, and the independent terms, as developed above, with the results:

$$\begin{aligned}
T_m &= \left[\frac{F_{b,p} \varepsilon_p}{F_{b,\infty}} T_p^4 + \frac{\alpha_b A_{\text{frontal}} E_s + \alpha_b A_b F_{b,p} \rho_p E_s}{2 \varepsilon_b A_b F_{b,\infty} \sigma} \right]^{\frac{1}{4}} = \\
&= \left[\frac{0.35 \cdot 0.6}{1} 288^4 + \frac{1 \cdot (\pi \cdot 1^2 / 4) \cdot 1370 + 1 \cdot \pi \cdot 1^2 \cdot 0.35 \cdot 0.3 \cdot 1370}{2 \cdot 1 \cdot \pi \cdot 1^2 \cdot 5.67 \cdot 10^{-8}} \right]^{\frac{1}{4}} = 275 \text{ K}
\end{aligned}$$

$$\varphi = \arctan \frac{\pi mc}{2 \varepsilon_b A_b F_{b,\infty} \sigma T_m^3 T_o} = \arctan \frac{\pi \cdot 50 \cdot 1000}{2 \cdot 1 \cdot \pi \cdot 1^2 \cdot 1 \cdot 5.67 \cdot 10^{-8} \cdot 275^3 \cdot 5429} = \arctan(3.9) = 1.32 \text{ rad}$$

$$\begin{aligned}
T_a &= \frac{\alpha_b A_{\text{frontal}} E_s + \alpha_b A_b F_{b,p} \rho_p E_s}{2 \left(\frac{2\pi mc \sin \varphi}{T_o} + \varepsilon_b A_b F_{b,\infty} \sigma 4 T_m^3 \right)} = \\
&= \frac{1 \cdot (\pi \cdot 1^2 / 4) \cdot 1370 + 1 \cdot \pi \cdot 1^2 \cdot 0.35 \cdot 0.3 \cdot 1370}{2 \left(\frac{2\pi \cdot 50 \cdot 1000 \cdot \sin(1.32)}{5429} + 1 \cdot \pi \cdot 1^2 \cdot 1 \cdot 5.67 \cdot 10^{-8} \cdot 4 \cdot 275^3 \right)} = 10.8 \text{ K}
\end{aligned}$$

The sinusoidal solution, $T(\phi) = 275 + 10.8 \cos(\phi - 1.32)$, in [K], is compared in Fig. E6.1 with the non-linear solution from Exercise 5, and the sinusoidal input here assumed with the real input.

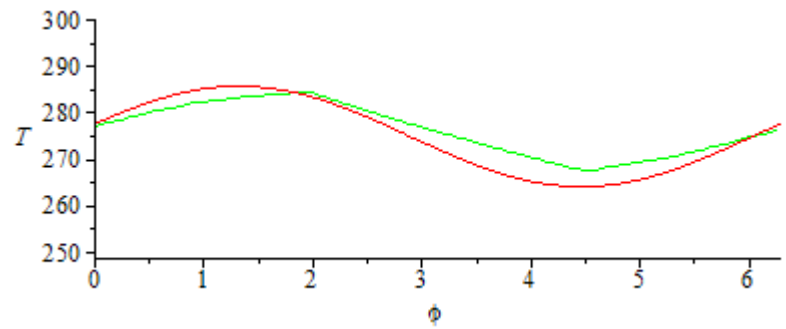


Fig. E6.1. Temperature evolution in the periodic state (T in [K] and ϕ in [rad]). Linear solution (in red) compared with non-linear one (green).

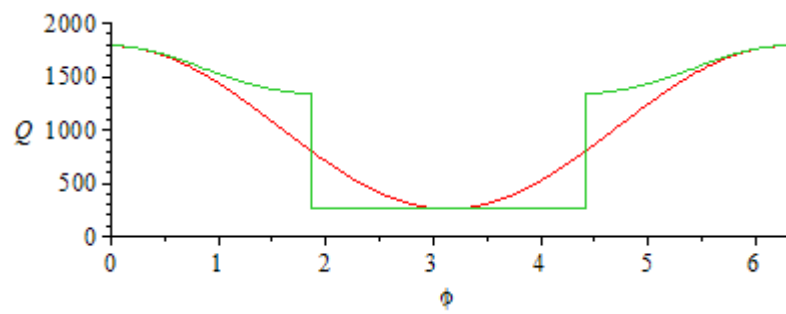


Fig. E6.2. Energy inputs along the orbit (Q in [W] and ϕ in [rad]). Linear solution (in red) compared with non-linear one (green); during eclipse, from $\phi=1.78$ to 4.41 , the only input is 259 W from planet emission.

Two nodes models

In one-node models (i.e. isothermal bodies) there are only energy exchanges with the environment (Sun, planet, and background). The next step in refining the thermal analysis is a model with two nodes in the spacecraft, i.e. a spatial discretization of the body in two parts at different temperatures (e.g. the shell and the main equipment box, a main box and an appendage...). The advantage of this two-node model is that it allows to consider heat transfer between the parts (by conduction through the joints, and radiation when they see each other, since convection will be absent in the vacuum of space, or even in pressurised boxes under microgravity).

The problem of finding the evolution of the two representative temperatures is solved by setting the energy balance for each part (1 and 2):

$$\left. \begin{aligned} m_1 c_1 \frac{dT_1}{dt} &= \dot{Q}_{s0,1} F_{e,1}(\phi) + \dot{Q}_{a0,1} F_{a,1}(\phi) + \dot{Q}_{p,1} + \dot{Q}_{\text{cond},2,1} + \dot{Q}_{\text{rad},2,1} - \dot{Q}_{\infty,1} \\ m_2 c_2 \frac{dT_2}{dt} &= \dot{Q}_{s0,2} F_{e,2}(\phi) + \dot{Q}_{a0,2} F_{a,2}(\phi) + \dot{Q}_{p,2} - \dot{Q}_{\text{cond},2,1} - \dot{Q}_{\text{rad},2,1} - \dot{Q}_{\infty,2} \end{aligned} \right\} \quad (26)$$

where each of the old-known terms (maximum solar input \dot{Q}_{s0} , maximum albedo input \dot{Q}_{a0} , planetary input \dot{Q}_p , and output to the environment \dot{Q}_{∞}) have the same formulation as above (only the numerical values change according to their respective data), and two new terms appear: the heat transfer by conduction from node 2 to node 1, $\dot{Q}_{\text{cond},2,1}$, and the heat transfer by radiation from node 2 to node 1, $\dot{Q}_{\text{rad},2,1}$. Notice that, instead of introducing in the second of (26) the heat transfer terms from 1 to 2, the negative of the corresponding terms from 2 to 1 have been used. The conductive and radiative heat exchange terms depend on temperatures, geometry and material properties, and are usually formulated as:

$$\dot{Q}_{\text{cond},2,1} = G_{2,1} (T_2 - T_1) \quad (27)$$

$$\dot{Q}_{\text{rad},2,1} = \sigma R_{2,1} (T_2^4 - T_1^4) \quad (28)$$

where $G_{2,1}$ and $R_{2,1}$ are known as the conductive and convective couplings between node 2 and node 1, which must be found by separately solving the specific thermal problem. The conductive coupling or thermal conductance, G , is often assumed to be a constant (dependent on material properties and geometry),

Spacecraft thermal modelling and testing

which may be computed by the electrical analogy method. The radiative coupling, R (sometimes including the constant σ), may depend in general on the temperatures (not only on T_1 and T_2 , but all others around), and must be computed by the exitance method, or by the Monte Carlo ray tracing method; however, in the case of blackbody surfaces this is also a constant, $R_{2,1}=A_2F_{2,1}$, as explained in [Heat transfer and thermal radiation modelling](#).

In normal practice, instead of the symbols G and R , GL (linear gain) and GR (radiative gain) are often used.

Exercise 7. Consider a circular-disc of radius $R_1=60$ cm, thickness $\delta_1=5$ mm, thermal capacity $C_1=500$ J/K, painted white on the front and black on the rear. The disc acts as a sunshield to a concentric spherical body of radius $R_2=0.5$ m, black-painted, which is at a distance $H=1$ m between centres, and has a thermal capacity $C_2=15$ kJ/K. Both objects are joined by a tubular pole made of aluminium with 1 cm external diameter and 0.3 mm wall thickness. The two objects are assumed to have high thermal conductivity and thus isothermal, constituting each one a node in the thermal problem. Find:

- The global thermal capacity of the pole, to justify the simplification to two nodes (disc 1, and sphere 2).
- All the view factors for the nodes.
- The conductive and radiative couplings between nodes if all the surfaces are considered blackbodies.
- The energy balance for the permanently aligned configuration Sun-disc-sphere in space (without nearby planets or moons), with the assumption of blackbodies.
- The network equations in the real grey-body case.

Sol.: The geometry is sketched in Fig. E7.1.

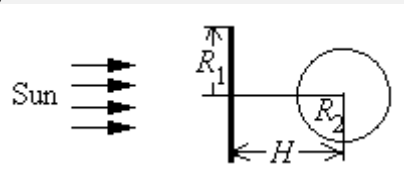


Fig. E7.1. Circular-disc sunshield of radius R_1 protecting from sunrays a concentric spherical body of radius $R_2 < R_1$ at a distance $H > R_2$ between centres.

- The global thermal capacity of the pole, to justify the simplification to two nodes (disc 1, and sphere 2).
With typical [aluminium properties](#), the global thermal capacity of the pole is $C=mc=\rho 2\pi R\delta Lc=2700\cdot 2\cdot \pi\cdot 0.005\cdot 0.0003\cdot 0.5\cdot 900=11.5$ J/K (the pole length is $L=H-R_2=1-0.5=0.5$ m), much lower than the thermal capacities of the other two parts, so that, considering its small dimensions, it is not retained as a new node, and the sole influence in the thermal analysis is the conductive coupling between the two nodes considered.
- All the view factors for the nodes.

From [View factor tabulations](#), we get, with $h\equiv H/R_1=1/0.6=1.67$ and $r_2\equiv R_2/R_1=0.5/0.6=0.83$:

$$F_{12} = 2r_2^2 \left(1 - \frac{1}{\sqrt{1 + \frac{1}{h^2}}} \right) = 2 \cdot 0.83^2 \left(1 - \frac{1}{\sqrt{1 + \frac{1}{1.67^2}}} \right) = 0.20$$

Notice that F_{12} is the fraction of energy emitted by one face of the disc (the face looking at the sphere, which we name ‘internal’) that is intersected by the sphere, i.e. really $F_{1i,2}$; the rest goes to the background, $F_{1i,\infty}=1-F_{1i,2}=0.80$. For the ‘external’ face of the disc, $F_{1e,\infty}=1$, since nothing blocks its view (recall that the Sun, and in fact any celestial body (planets and moons), is not considered as a normal object with which heat is transferred, but only as an energy input. Concerning the sphere, the generic reciprocity relation $A_1F_{12}=A_2F_{21}$ allows to find $F_{2,1i}=\pi R_1^2 F_{1i,2}/(4\pi R_2^2)=\pi \cdot 0.6^2 \cdot 0.20/(4 \cdot \pi \cdot 0.5^2)=0.072$, and $F_{2,\infty}=1-F_{2,1i}=0.93$.

c) The conductive and radiative couplings between nodes if all the surfaces are considered blackbodies.

Thermal conduction between disc and sphere is through the aluminium pole cross-section of area $A=2\pi R\delta=2 \cdot \pi \cdot 0.005 \cdot 0.0003=9.4 \cdot 10^{-6} \text{ m}^2$. The heat transfer is:

$$\dot{Q}_{\text{cond},2,1} = G_{2,1} (T_2 - T_1) = kA \frac{T_2 - T_1}{L} \rightarrow G_{2,1} = \frac{kA}{L} = \frac{200 \cdot 9.4 \cdot 10^{-6}}{0.5} = 3.8 \cdot 10^{-3} \frac{\text{W}}{\text{K}}$$

where the pole length is $L=H-R_2=1-0.5=0.5 \text{ m}$.

The radiative couplings in the case of blackbodies coincide with the area times the view factor, i.e.,

$$\dot{Q}_{\text{rad},2,1} = \sigma R_{2,1} (T_2^4 - T_1^4) = \sigma A_2 F_{2,1} (T_2^4 - T_1^4)$$

d) The energy balance for the permanently aligned configuration Sun-disc-sphere in space (without nearby planets or moons), with the assumption of blackbodies.

Node 1, of thermal capacity C_1 and temperature $T_1(t)$, gets a solar power $\dot{Q}_{s,1e} = \alpha_{1e} A_{1e} E_s = 1 \cdot \pi \cdot 0.6^2 \cdot 1360 = 1550 \text{ W}$ (310 W with a white paint of $a=0.2$) at its ‘external’ surface, A_{1e} . It also gets a power $\dot{Q}_{\text{cond},2,1} = G_{2,1} (T_2 - T_1)$ by conduction through the pole, and a radiation power $\dot{Q}_{\text{rad},2,1} = \sigma A_{1i} F_{1i,2} (T_2^4 - T_1^4)$ directly from node 2. But, apart from node 2 (the sphere), node 1 is exchanging a heat power $\sigma A_{1i} F_{1i,\infty} (T_\infty^4 - T_1^4)$ with the background seen by the ‘internal’ surface ($F_{1i,\infty}=0.80$) and a heat power $\sigma A_{1e} F_{1e,\infty} (T_\infty^4 - T_1^4)$ with the background seen by the ‘external’ surface ($F_{1e,\infty}=1$). The energy balance for node 1 is thence:

$$C_1 \frac{dT_1}{dt} = A_{1e} E_s + G_{2,1} (T_2 - T_1) + \sigma A_{1i} F_{1i,2} (T_2^4 - T_1^4) + \sigma A_{1i} F_{1i,\infty} (T_\infty^4 - T_1^4) + \sigma A_{1e} F_{1e,\infty} (T_\infty^4 - T_1^4)$$

For node 2 is entirely similar, with the simplification that it only has one continuous face (the sphere has uniform properties, contrary to the disc), so that the energy balance is:

$$C_2 \frac{dT_2}{dt} = 0 - G_{2,1}(T_2 - T_1) - \sigma A_{1i} F_{1i,2} (T_2^4 - T_1^4) + \sigma A_2 F_{2,\infty} (T_\infty^4 - T_2^4)$$

where now there is no solar input, the heat conduction from node 1 is $\dot{Q}_{\text{cond},1,2} = G_{1,2}(T_1 - T_2) = -\dot{Q}_{\text{cond},2,1} = -G_{2,1}(T_2 - T_1)$, the heat radiation from node 1 is $\dot{Q}_{\text{rad},1,2} = \sigma A_2 F_{2,1i} (T_1^4 - T_2^4) = -\dot{Q}_{\text{rad},2,1} = -\sigma A_{1i} F_{1i,2} (T_2^4 - T_1^4)$, and the heat radiation with the background is $\sigma A_2 F_{2,\infty} (T_\infty^4 - T_2^4)$, with $F_{2,\infty}=0.93$.

Substitution of numerical values (with $T_\infty=2.7 \text{ K} \approx 0$) yields:

$$500 \frac{dT_1}{dt} = 1550 + 3.8 \cdot 10^{-3} \cdot (T_2 - T_1) + 12.8 \cdot 10^{-9} \cdot (T_2^4 - T_1^4) - 51.3 \cdot 10^{-9} \cdot T_1^4 - 64.1 \cdot 10^{-9} \cdot T_1^4$$

$$15 \cdot 10^3 \frac{dT_2}{dt} = -3.8 \cdot 10^{-3} \cdot (T_2 - T_1) - 12.8 \cdot 10^{-9} \cdot (T_2^4 - T_1^4) - 166 \cdot T_2^4$$

Numerical integration from an arbitrary initial state of $T_1(0)=T_2(0)=300 \text{ K}$ yields the results presented in Fig. E7.2. The final steady state can be found by solving the above equations with $dT/dt=0$, with the result $T_1(\infty)=332 \text{ K}$, $T_2(\infty)=172 \text{ K}$.

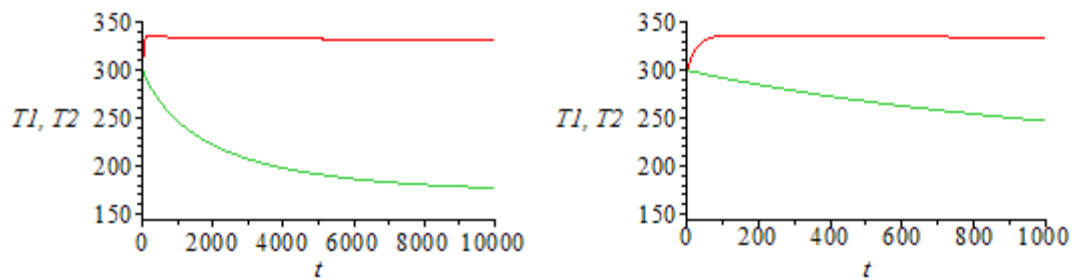


Fig. E7.2. a) Temperature evolution of the disc (node 1, in red) and the sphere (node 2, in green), assumed blackbodies, from an arbitrary initial conditions $T_1(0)=T_2(0)=300 \text{ K}$. B) Initial details. T in [K] and t in [s].

Notice in Fig. E7.2 the different transient times of the nodes, due to different thermal capacities; node 1 has very low thermal inertia and equilibrates in a hundred of seconds, while node 2 takes several hours to equilibrate. In fact, node 2 is initially so hot that node 1 first stabilises to 336 K before finally reaching the 332 K in the long run.

e) The network equations in the real grey-body case.

Now, due to the difficulty in formulating the radiation heat transfer, instead of writing the energy balance equation as $C_i dT_i/dt = \dot{W}_i + \dot{Q}_{\text{cond},i} + \dot{Q}_{\text{rad},i}$, it is better to set it as $\dot{Q}_{\text{rad},i} = C_i dT_i/dt - \dot{W}_i - \dot{Q}_{\text{cond},i}$. Besides, one must choose one node at each ‘uniform’ surface in the radiative enclosure, so that we are forced to separate node 1 in node 1e and node 1i, each with half the total thermal capacity and conductively connected through a high enough conductance to make the difference in temperature negligible. The equations to solve are, at each node i (see [The network method, in Heat transfer and thermal radiation modelling](#)):

$$\dot{Q}_{\text{rad},i} = \frac{M_i - M_{i,\text{bb}}}{\frac{1 - \varepsilon_i}{A_i \varepsilon_i}} = \sum_j \frac{M_j - M_i}{\frac{1}{A_i F_{i,j}}} = C_i \frac{dT_i}{dt} - \dot{W}_i - \dot{Q}_{\text{cond},i}$$

which in our case of three nodes, and leaving out the $\dot{Q}_{\text{rad},i}$ -variables, become:

$$\text{node 1e: } \frac{M_{1e} - M_{1e,\text{bb}}}{\frac{1 - \varepsilon_{1e}}{A_{1e} \varepsilon_{1e}}} = \frac{M_\infty - M_{1e}}{A_{1e} F_{1e,\infty}} = C_{1e} \frac{dT_{1e}}{dt} - \alpha_{s,1e} A_{1e} E_s - K_{1e,1i} (T_{1i} - T_{1e})$$

$$\text{node 1i: } \frac{M_{1i} - M_{1i,\text{bb}}}{\frac{1 - \varepsilon_{1i}}{A_{1i} \varepsilon_{1i}}} = \frac{M_\infty - M_{1i}}{A_{1i} F_{1i,\infty}} + \frac{M_2 - M_{1i}}{A_{1i} F_{1i,2}} = C_{1i} \frac{dT_{1i}}{dt} - K_{1e,1i} (T_{1e} - T_{1i}) - K_{2,1i} (T_2 - T_{1i})$$

$$\text{node 2: } \frac{M_2 - M_{2,\text{bb}}}{\frac{1 - \varepsilon_2}{A_2 \varepsilon_2}} = \frac{M_\infty - M_2}{A_2 F_{2,\infty}} + \frac{M_{1i} - M_2}{A_2 F_{2,1}} = C_2 \frac{dT_2}{dt} - K_{2,1i} (T_{1i} - T_2)$$

which is a system of 6 equations (6 equal sign) with 6 unknown (two at each node): M_{1e} , $M_{1e,\text{bb}}$, M_{1i} , $M_{1i,\text{bb}}$, M_2 , $M_{2,\text{bb}}$, since temperatures are directly related to blackbody exitances by $M_{\text{bb}} = \sigma T^4$. Notice how solar energy is treated separately from IR radiation, as dissipated power, $\dot{W}_{1e} = \alpha_{s,1e} A_{1e} E_s$. This system is most often interpreted and written according to an electrical analogy as shown in Fig. E7.3, where one sets 6 variable nets (one per ‘voltage’ M) plus an additional one for the ‘ground voltage’ $M_\infty = \sigma T_\infty^4 \approx 0$, with interconnecting radiative resistances according to the denominators in the equations above (notice there is no radiative coupling between the two sides of the disc), and local energy sinks corresponding to the right side of the equations above.

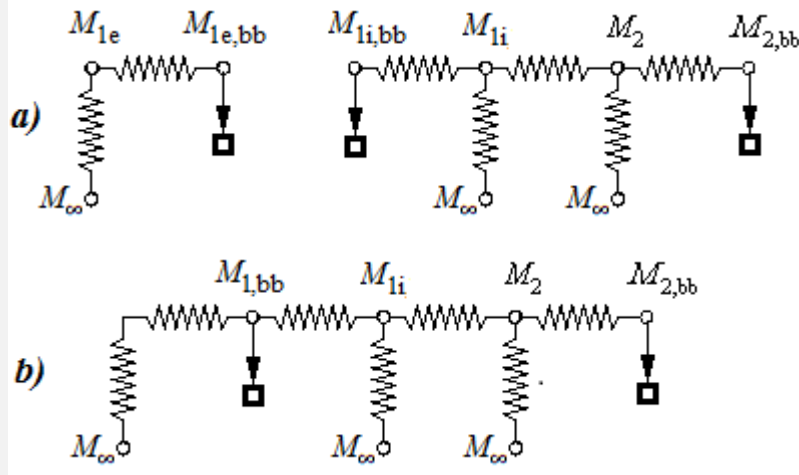


Fig. E7.3. a) Initial electrical-analogy circuit, and a network simplification.

The energy flow balance at each of the nets ($M_{1e}, M_{1e,\text{bb}}, M_{1i}, M_{1i,\text{bb}}, M_2, M_{2,\text{bb}}$) is, respectively:

$$\text{net } M_{1e}: \frac{M_\infty - M_{1e}}{A_{1e} F_{1e,\infty}} + \frac{M_{1e,\text{bb}} - M_{1e}}{A_{1e} \varepsilon_{1e}} = 0$$

$$\begin{aligned} \text{net } M_{1e,bb}: \quad & \frac{M_{1e} - M_{1e,bb}}{1 - \varepsilon_{1e}} = C_{1e} \frac{dT_{1e}}{dt} - \alpha_{s,1e} A_{1e} E_s - G_{1e,1i} (T_{1i} - T_{1e}) \\ & \frac{A_{1e} \varepsilon_{1e}}{A_{1e} \varepsilon_{1e}} \\ \text{net } M_{1i,bb}: \quad & \frac{M_{1i} - M_{1i,bb}}{1 - \varepsilon_{1i}} = C_{1i} \frac{dT_{1i}}{dt} - G_{1e,1i} (T_{1e} - T_{1i}) - G_{2,1i} (T_2 - T_{1i}) \\ & \frac{A_{1i} \varepsilon_{1i}}{A_{1i} \varepsilon_{1i}} \\ \text{net } M_{1i}: \quad & \frac{M_{1i,bb} - M_{1i}}{1 - \varepsilon_{1i}} + \frac{M_2 - M_{1i}}{1} + \frac{M_\infty - M_{1i}}{1} = 0 \\ & \frac{A_{1i} \varepsilon_{1i}}{A_{1i} \varepsilon_{1i}} \quad \frac{A_{1i} F_{1i,2}}{A_{1i} F_{1i,2}} \quad \frac{A_{1i} F_{1i,\infty}}{A_{1i} F_{1i,\infty}} \\ \text{net } M_2: \quad & \frac{M_{1i} - M_2}{1} + \frac{M_{2,bb} - M_2}{1 - \varepsilon_2} + \frac{M_\infty - M_2}{1} = 0 \\ & \frac{A_2 F_{2,1}}{A_2 F_{2,1}} \quad \frac{A_2 \varepsilon_2}{A_2 \varepsilon_2} \quad \frac{A_2 F_{2,\infty}}{A_2 F_{2,\infty}} \\ \text{net } M_{2bb}: \quad & \frac{M_2 - M_{2,bb}}{1 - \varepsilon_2} = C_2 \frac{dT_2}{dt} - G_{2,1i} (T_{1i} - T_2) \\ & \frac{A_2 \varepsilon_2}{A_2 \varepsilon_2} \end{aligned}$$

The simplification of this initial electrical-analogy circuit shown in Fig. E7.3 reduces to system to 4 equation with 4 unknowns ($M_{1,bb}, M_{1i}, M_2, M_{2,bb}$):

$$\begin{aligned} \text{net } M_{1bb}: \quad & \frac{M_\infty - M_{1,bb}}{1} + \frac{M_{1i} - M_{1,bb}}{1 - \varepsilon_{1e}} = C_1 \frac{dT_1}{dt} - \alpha_{s,1e} A_{1e} E_s - G_{2,1} (T_2 - T_1) \\ & \frac{A_{1e} F_{1e,\infty}}{A_{1e} F_{1e,\infty}} + \frac{A_{1e} \varepsilon_{1e}}{A_{1e} \varepsilon_{1e}} \quad \frac{A_{1i} \varepsilon_{1i}}{A_{1i} \varepsilon_{1i}} \\ \text{net } M_{1i}: \quad & \frac{M_{1,bb} - M_{1i}}{1 - \varepsilon_{1i}} + \frac{M_2 - M_{1i}}{1} + \frac{M_\infty - M_{1i}}{1} = 0 \\ & \frac{A_{1i} \varepsilon_{1i}}{A_{1i} \varepsilon_{1i}} \quad \frac{A_{1i} F_{1i,2}}{A_{1i} F_{1i,2}} \quad \frac{A_{1i} F_{1i,\infty}}{A_{1i} F_{1i,\infty}} \\ \text{net } M_2: \quad & \frac{M_{1i} - M_2}{1} + \frac{M_{2,bb} - M_2}{1 - \varepsilon_2} + \frac{M_\infty - M_2}{1} = 0 \\ & \frac{A_2 F_{2,1}}{A_2 F_{2,1}} \quad \frac{A_2 \varepsilon_2}{A_2 \varepsilon_2} \quad \frac{A_2 F_{2,\infty}}{A_2 F_{2,\infty}} \\ \text{net } M_{2bb}: \quad & \frac{M_2 - M_{2,bb}}{1 - \varepsilon_2} = C_2 \frac{dT_2}{dt} - G_{2,1} (T_1 - T_2) \\ & \frac{A_2 \varepsilon_2}{A_2 \varepsilon_2} \end{aligned}$$

And we can extract the intermediate variables M_2 and M_{1i} from the last two equations and substitute in the other two, to leave a system of 2 equations with 2 unknowns (T_1 and T_2), which have to be solved numerically because of the non-linearity. The result is shown in Fig. E7.4.

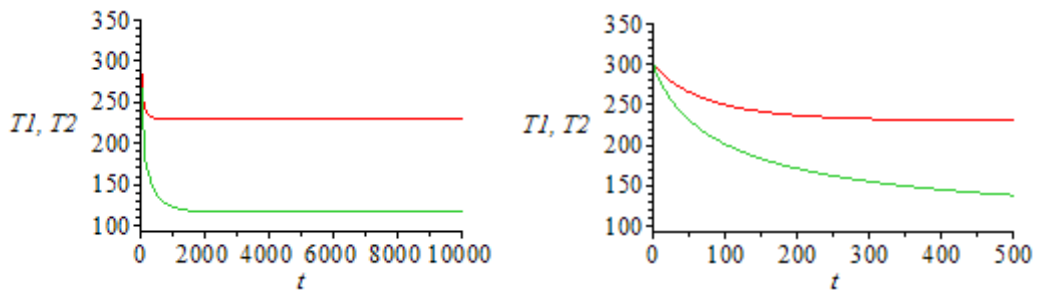


Fig. E7.4. a) Temperature evolution of the disc (node 1, in red) and the sphere (node 2, in green), from an arbitrary initial conditions $T_1(0)=T_2(0)=300$ K. B) Initial details. T in [K] and t in [s]. Real thermo-optical properties.

Analytical two-nodes sinusoidal solution

As for one-node models developed above, we try to take advantage of the fact that, for low altitude orbits, the input thermal loads follow an up-and-down pattern (high gains when under sunshine, low gains under eclipse), so that a cosine modulation over the average may be a suitable first approximation. Moreover, as temperature variations along the orbit are not so great (a few tens of kelvin around 300 K or so), we may linearize the problem and get an analytical result.

In the one-node case, the energy equation (with solar input, albedo input, planetary input, and IR output) was:

$$mc \frac{dT}{dt} = \dot{Q}_{s0} F_e(\phi) + \dot{Q}_{a0} F_a(\phi) + \dot{Q}_p - \dot{Q}_\infty \quad (29)$$

Now with two nodes we can introduce conductive and radiative couplings between them, to better model the real behaviour when the assumption of same temperature for the whole spacecraft is untenable, as in Exercise 7 above. We intend to make the same smoothing in the loads as before, i.e. setting the eclipse and albedo factors $F_e = F_a = (1 + \cos\phi)/2$. Now the energy balance equation at each node is:

$$\left. \begin{aligned} m_1 c_1 \frac{dT_1}{dt} &= \dot{Q}_{s0,1} F_{e,1}(\phi) + \dot{Q}_{a0,1} F_{a,1}(\phi) + \dot{Q}_{p,1} + \dot{Q}_{cond2,1} + \dot{Q}_{rad2,1} - \dot{Q}_{1,\infty} \\ m_2 c_2 \frac{dT_2}{dt} &= \dot{Q}_{s0,2} F_{e,2}(\phi) + \dot{Q}_{a0,2} F_{a,2}(\phi) + \dot{Q}_{p,2} - \dot{Q}_{cond2,1} - \dot{Q}_{rad2,1} - \dot{Q}_{2,\infty} \end{aligned} \right\} \quad (30)$$

and the answer we are looking for is:

$$\left. \begin{aligned} T_1(\phi) &= T_{1m} + T_{1a} \cos(\phi - \phi_1) \\ T_2(\phi) &= T_{2m} + T_{2a} \cos(\phi - \phi_2) \end{aligned} \right\} \quad (31)$$

When we expand all terms in (30) with this sinusoidal model, i.e.. with:

$$\left. \begin{aligned} \dot{Q}_{s0,1} F_{e,1}(\phi) + \dot{Q}_{a0,1} F_{a,1}(\phi) + \dot{Q}_{p,1} &= \left(\alpha_1 A_{1,frontal} E_s + \alpha_1 A_1 F_{1,p} \rho_p E_s \right) \frac{1 + \cos(\phi)}{2} + \varepsilon_1 A_1 F_{1,p} \varepsilon_p \sigma T_p^4 \\ \dot{Q}_{cond2,1} &= G_{12} (T_2 - T_1) = G_{12} \left[T_{2m} + T_{2a} \cos(\phi - \phi_2) - T_{1m} - T_{1a} \cos(\phi - \phi_1) \right] \\ \dot{Q}_{rad2,1} &= \sigma A_1 F_{12} (T_2^4 - T_1^4) = \sigma A_1 F_{12} \left[T_{2m}^4 + 4T_{2m}^3 T_{2a} \cos(\phi - \phi_2) - T_{1m}^4 - 4T_{1m}^3 T_{1a} \cos(\phi - \phi_1) \right] \\ \dot{Q}_{1,\infty} &= \varepsilon_1 A_1 F_{1,\infty} \sigma T_1^4 = \varepsilon_1 A_1 F_{1,\infty} \sigma \left[T_{1m}^4 + 4T_{1m}^3 T_{1a} \cos(\phi - \phi_1) \right] \end{aligned} \right\} \quad (32)$$

and we group in the independent-variable orthogonal functions, we get two equations of the form:

$$\left. \begin{aligned} C_{10} + C_{1c} \cos\phi + C_{1s} \sin\phi &= 0 \\ C_{20} + C_{2c} \cos\phi + C_{2s} \sin\phi &= 0 \end{aligned} \right\} \quad (33)$$

where the independent-term coefficients (C_{10} and C_{20}), the cosine coefficients (C_{1c} and C_{2c}), and the sine coefficients (C_{1s} and C_{2s}), are dependent on the two-node geometry and material data, and on the 6 unknowns we introduced in (31) ($T_{1m}, T_{1a}, \varphi_1, T_{2m}, T_{2a}, \varphi_2$), which are obtained by solving the 6 equations $C_{10}=C_{20}=C_{1c}=C_{2c}=C_{1s}=C_{2s}=0$. As for the one-node case, the orbit mean temperatures, T_{1m} and T_{2m} , could be obtained by solving (30) with the left-hand sides equal zero. The conclusions are similar to the one-node case: the time-lag in the response (φ_1, φ_2) is proportional to thermal capacity, and increases also with shorter orbit periods; besides, in the two-node case, the difference in time lag between nodes also increases with higher thermal resistances (conductive and radiative) between them.

A more detailed analysis can be found in Pérez-Grande et al., *Applied Thermal Engineering* 29 (2009) 2567–2573.

Multi-node models

Only the most crude spacecraft thermal discretization can be solved by hand, since each panel usually yields two nodes (one at each face), and models with more than a few nodes are cumbersome to deal with manually.

Automated and semi-automated modelling tools are available to solve hundreds and thousands of nodes, but this is not a panacea: the burden of solving the node equations is transferred to the burden of dealing with myriads of numbers from which meaningful data are difficult to extract. Recourse is made to computer graphics to plot maps of temperatures and temperature strip-charts, but if the geometry is not simple, the visualization may be entangled.

And one of the key problems when massive manual data entry is involved is how to guarantee the data input is free of typing mistakes.

A key point to remember when actually doing the mathematical modelling of thermal problems is that it is nonsense to start demanding great accuracy in the solution when there is not such accuracy in the input parameters and constraints. Without specific experimental tests, there are big uncertainties even in materials properties, like thermal conductivity of metal alloys, entrance and blocking effects in convection, and particularly uncertainty in thermo-optical properties.

Node selection

The minimum number of nodes to achieve reasonable thermal accuracy should be established; debugging of input data, computing resources, and handling of output data, all grow with the number of nodes.

The thermal problem must direct node selection. Geometrical data It is nonsense using many nodes just to have a smooth visualization; smoothing may be done afterwards by computer graphics on discrete computed data.

It is also nonsense using data with say 10% uncertainty in value (e.g. thermo-optical properties), and pretending five significant digits in node temperature.

It is important to label nodes using short but meaningful names, and group nodes within component submodels. Table 1 gives an idea of how a tabulation of node descriptions may look like.

Table 1. Example of node description matrix.

Node #	description	label	type	Coordinates ^{a)}	Accep. T -range [K]	P [W] ^{b)}	mc [J/K]	T_{fix} [K]
999	deep space	BGRN	b.c.	NA	NA		∞	2.7
998	sun	SUN	b.c.	NA	NA		∞	5800
997	planet	PL	b.c.	NA	NA		∞	298
101	solar panel 1	SP1	ext.	xyz=???, xyz=...	200..400	3	5000	?
201	ext. sat face 1	SF1	ext.	xyz=???, xyz=...	200..400		1000	?
202	int. sat face 1	SF2	int.	xyz=???, xyz=...	200..400			?
400	battery 1	BT1	int.	xyz=???, xyz=...	270..330	10	10 000	?
...								

a) A centred body reference is used; for nodes with geometry or position varying with time, a time series must be specified. NA, not applicable.

b) P stands for dissipated power, not for electrical transmission; it is usual for nodes to have electrical dissipation varying with time, and thence a time series must be specified.

Nodal equations

The thermal energy balance for a generic node i in a N -node spacecraft discretization, may be written as $C_i dT_i/dt = \Sigma \dot{Q}_{ij, \text{input}}$, where only heat inputs appear because electrical and electromagnetic dissipation are taken as heat inputs, and the electrical balance is analysed aside (as explained above under Solar cell effect). A more detailed thermal balance, where the different heat inputs and outputs are shown, and time is already discretized, takes the form:

$$C_i \frac{T_i^+ - T_i}{\Delta t} = \sum_{j=0}^N \dot{Q}_{ij} = \dot{Q}_{\text{int},i} + \dot{Q}_{\text{ext},i} + \sum_{\substack{j=1 \\ j \neq i}}^N \dot{Q}_{ij} = \dot{Q}_{\text{dis},i} + \dot{Q}_{\text{s,th},i} + \dot{Q}_{\text{a,th},i} + \dot{Q}_{\text{p},i} - \dot{Q}_{\infty,i} + \sum_{\substack{j=1 \\ j \neq i}}^N \dot{Q}_{\text{con},ij} + \sum_{\substack{j=1 \\ j \neq i}}^N \dot{Q}_{\text{rad},ij} \quad (34)$$

where C_i is the overall thermal capacity of node i , T_i^+ and T_i are node i temperature after and before advancing a Δt in time (Euler discretization of time). Notice that, in many computer packages, two external nodes are added, the planet (or moon) and the background, and then there is no explicit infrared-input-from-planet term, $\dot{Q}_{\text{p},i}$, and node-own-emission term, $\dot{Q}_{\infty,i}$, because they are included in the summation for node radiation exchanges.

The ‘heat input’ due to electrical dissipation within the node, $\dot{Q}_{\text{dis},i}$ is a mission-operation data, although in the case of heaters and other active elements of STC can be under control of the thermal designer.

The solar ‘heat input’, $\dot{Q}_{\text{s,th},i}$ (really electromagnetic dissipation) is of the form:

$$\dot{Q}_{\text{s,th},i} = (\alpha_s - \eta F_{\text{pg}}) E_s A_{\text{frontal}}(t) F_c(t) \quad (35)$$

where only thermal solar absorption must be accounted for (in the case of nodes with solar cells, this is total solar absorption, α_s , minus cell electrical efficiency, η , times the packaging factor, F_{pg}), E_s is solar irradiation normal to Sun direction, A_{frontal} the node projected area perpendicular to Sun rays ($A_{\text{frontal}}=A\cos\beta$ for a planar patch tilted an angle β ; its time dependence is fixed by orbital mechanics and spacecraft attitude control), and F_e an eclipse factor (equal to 1 if the node is sunlit, or 0 if at shadow; its time dependence is fixed by orbital mechanics).

The albedo ‘heat input’, $\dot{Q}_{a,th,i}$ (really electromagnetic dissipation similar to solar input) takes the form:

$$\dot{Q}_{a,th,i} = (\alpha_s - \eta F_{pg}) \rho_p E_s A_i F_{i,p}(t) F_a(t) \quad (36)$$

where ρ_p is planet albedo (i.e. solar reflectance), $A_i F_{i,p}=A_p F_{p,i}$ is the part of the planet reflected power falling on A_i (the view factor $F_{i,p}$ is tabulated for most simple geometries), and F_a is an albedo factor accounting for the planet phase seen from the spacecraft, equals 1 at the subsolar point, 0 at eclipse, and the following interpolation function for partially lit planet or moon (explained above under Albedo effect):

$$F_a = \left(\frac{1 + \cos\phi}{2} \right)^2 \left[1 - \left(\frac{\phi}{\phi_{es}} \right)^2 \right] \cos\beta F_e, \quad F_e = \begin{cases} 1 & \text{if } -\phi_{es} < \phi < \phi_{es} \\ 0 & \text{otherwise} \end{cases} \quad (37)$$

where β is the orbit solar angle. The planet ‘heat input’, $\dot{Q}_{p,i}$ (here not properly a heat-term because it is not the net energy exchange due to temperature difference) takes the form:

$$\dot{Q}_{p,i} = \varepsilon_i A_i F_{i,p}(t) \varepsilon_p \sigma T_i^4 \quad (38)$$

where ε_i is the node absorptance in the IR band (equal to its emissivity), $A_i F_{i,p}=A_p F_{p,i}$ is the part of the planet emitted power falling on A_i , ε_p is planet emissivity, σ the Stefan-Boltzmann constant, and T_i is the node temperature.

The node ‘heat output’ to the environment, $\dot{Q}_{\infty,i}$ (it is not properly heat because it is not the net energy exchange due to temperature difference, although it can be so considered if the background temperature, $T_\infty=2.7$ K, is neglected in comparison with node temperature, or really their fourth power), takes the form:

$$\dot{Q}_{\infty,i} = \varepsilon_i A_i F_{i,\infty}(t) \sigma T_i^4 \quad (39)$$

where $F_{i,\infty}$ is the view factor from node i to the spacecraft environment including the background empty space, the planet or moon, and the solar disc, because only inputs from the latter were accounted for in the ‘heat input’ terms.

Heat transfer between spacecraft nodes, the conductive and radiative couplings, is treated below.

Node couplings

The heat input (net value) to node i by conduction and possibly convection, $\dot{Q}_{\text{con},i}$ in (33), coming from the other nodes, can always be written as:

$$\dot{Q}_{\text{con},i} = \sum_{\substack{j=1 \\ j \neq i}}^N \dot{Q}_{\text{con},ij} = \sum_{\substack{j=1 \\ j \neq i}}^N G_{ij} (T_j - T_i) = \sum_{\substack{j=1 \\ j \neq i}}^N GL_{ij} (T_j - T_i) = \sum_{\substack{j=1 \\ j \neq i}}^N \frac{k_{ij,\text{eff}} A_{ij,\text{eff}}}{L_{ij,\text{eff}}} (T_j - T_i) \quad (40)$$

where G_{ij} (often named GL_{ij}) is the conductance between nodes (or conduction coupling), which can be stated as an effective conductivity of the materials implied ($k_{ij,\text{eff}}$), times an effective heat-flow area ($A_{ij,\text{eff}}$), divided by an effective distance between nodes ($L_{ij,\text{eff}}$). The computation of the conductive couplings, C_{ij} , must be done manually aside for most commercial thermal analysis packages, what means an additional burden for the data input.

The heat input (net value) to node i by radiation, $\dot{Q}_{\text{rad},i}$, coming from the other nodes, may be written as:

$$\dot{Q}_{\text{rad},i} = \sum_{\substack{j=1 \\ j \neq i}}^N \dot{Q}_{\text{rad},ij} = \sum_{\substack{j=1 \\ j \neq i}}^N \sigma R_{ij} (T_j^4 - T_i^4) = \sum_{\substack{j=1 \\ j \neq i}}^N \sigma GR_{ij} (T_j^4 - T_i^4) \quad (41)$$

where R_{ij} (often named GR_{ij}) is the radiative coupling, which coincides with the view factor times area in the case of all node surfaces being blackbodies, but which must be obtained by solving the node-exitances (radiosities) from the network model explained in [The network method, in Heat transfer and thermal radiation modelling](#).

A node matrix of $N \times N$ thermal couplings amongst the N nodes can be filled containing all the data, taking advantage of the symmetry in node interaction, $G_{ij}=G_{ji}$ and $R_{ij}=R_{ji}$, and thermal capacities be included in the diagonal; e.g.:

- Radiative couplings between node i and node j in the upper triangular side of the matrix.
- Thermal capacities of each node i in the diagonal of the matrix.
- Conductive couplings between node i and node j in the lower triangular side of the matrix.

Table 2. Matrix of thermal couplings and thermal capacities.

$i \setminus j$	1	2	3	4	...
1	$m_1 c_1$	R_{12}	R_{13}		
2	G_{21}	$m_2 c_2$			
3	G_{31}				
4					
...					

Exercise 8. [An 11-node model of a lunar satellite box \(.doc\)](#).

Numerical simulation

Thermal analyses of large-scale spacecraft are currently performed with a variety of industry standard programs, which can be grouped in:

Spacecraft thermal modelling and testing

- Radiation exchange packages: ESARAD, TRASYS, THERMICA, SINDARadCAD...
- Lumped finite-difference thermal balance packages: ESATAN, SINDA, ...
- Finite-element thermal balance packages: NASTRAN, COSMOS, ANSYS, FLOTHERM...

ESATAN-TMS (ESA Thermal Analysis Network –Thermal Modelling Suite), developed by ITP Engines UK, formerly Aston Power, under ESA contract since the late 1970s, is the most used numerical simulation package in Europe. It is composed of the following components (further details can be found in <http://www.itp-engines.co.uk/>):

- *Workbench* is an integrated environment with full pre- and post-processing capabilities, providing geometry modelling, visualisation, reporting, and analysis case control.
- *Thermal* (ESATAN) is the nodal equation solver.
- *ThermNV* is a tool for the visualisation of a thermal network including pre/post-processing of model data.
- *ThermXL* is a spread-sheet add-in to Microsoft Excel for solving thermal analysis problems and is designed to fulfil the need for rapid turn-around of system level or simple "what-if" (parametric) type analyses.
- *Fluids* (formerly FHTS) is an extension to ESATAN providing single and two-phase thermo-hydraulic modelling of piped fluid networks.
- *Radiative* (formerly ESARAD, coming from an early program VWHEAT) is dedicated to surface-to-surface extended radiative calculation with support for specular and transparent surfaces.
- *Mission* is dedicated to the analysis of orbiting and interplanetary bodies, with solar and planet heating.

On the other hand, the combinations SINDA-TRASYS is the most used finite-differencing thermal and fluid network analyzer in the USA. The MSC Sinda family of thermal design products comprises:

- *MSC Sinda Analyzer* is the finite-differences nodal equation solver. It originated in the 1960's at Chrysler Aerospace as CINDA code, and was adapted by NASA in the 1970s.
- *MSC Sinda for Patran* is a converter from MSC Sinda to Patran or MSC Nastran, for finite element analysis (FEA).
- *SindaRadCAD* is dedicated to radiative couplings.
- *SindaFloCAD* (or *SINDA/FLUINT*) is an extension for heat transfer design with fluid flow.
- *TRASYS* (Thermal Radiation Analyzer SYStem, originally released as part of the NASA Cosmic collection), computes the total thermal radiation environment for a spacecraft in orbit.

The THERMICA Suite (from EADS Astrium, since 1988) is composed of two main packages:

- *THERMICA*, the pre- and post-processor to translate the geometrical model and its environment into a mathematical model by computing all thermal fluxes and couplings using a Monte-Carlo ray-tracing technique for thermal radiation simulation. Also distributed as MSC THERMICA.
- *THERMISOL*, the THERMICA solver based on ESATAN. But THERMICA is also compatible with MSC Sinda Analyzer.

EcosimPro, developed since 1989 by Empresarios Agrupados, under ESA contract, is a numerical simulator of generic dynamic system represented by differential-algebraic equations. THERMAL, a standard library supplied with EcosimPro, helps predicting temperature distributions and heat flows using the thermal network method.

Finite differences method vs. Finite elements method

An advantage of finite element methods is that the same program can be used for thermal analysis and for structural analysis. Heat transfer, particularly in radiation, is highly non-linear and thermal analysts tend to use as few thermal elements (nodes) as possible to reduce computing effort and cost. Similar restrictions do not apply to structural finite element program, and thus thermal and structural models will not be compatible for joint analysis with typical ratios of thermal to structural nodes of 1 to 20..50 being encountered. In practice this mismatch will burden the structural analyst, when asked to calculate thermal distortions, with the effort of interpolating temperatures in his structural model. On the other hand a thermal analyst may spend a disproportionate amount of time evaluating conductions for a model which only schematically matches a real structure.

Stochastic modelling and spacecraft thermal analysis

The thermal analysis of spacecraft in orbit is currently a computationally expensive task. Monte Carlo ray-tracing is typically used to determine the parameters for the radiative heat transfer from the Sun and planet, and between different parts of the spacecraft. These parameters are then added to a mathematical model representing the conductive heat transfer, and iterative finite difference solvers are used to calculate temperatures within the spacecraft. Finding, for instance, the critical design cases (hottest, coldest, etc.) may involve running many parametric studies. In general, any optimisation process for the spacecraft design, or the correlation of the spacecraft model against test data, will require further parametric studies. Stochastic techniques involve applying probability functions to select values for these variables at random from a given range, and using statistical methods to determine the influence of the variable and the accuracy of the result. Software tools now exist to automate the process of selecting the values for the variables, and providing statistical feedback to the engineer to help arrive at the important analysis cases using fewer parametric runs than traditional methods.

Analysis of results

The analysis of the results may be quite different in the case of a closed analytical solution than for the case of a numerical solution. In the last case, the interpretation of the numerical solution to judge its validity, accuracy and sensitivity to input parameters can be quite involved. The direct solution usually gives just the set of values of the function at the nodes, what is difficult to grasp for humans in raw format (a huge list of numbers or, for regular meshes, a matrix). Some basic post-processing tools are needed for:

- Visualization of the function by graphic display upon the geometry or at user-selected cuttings. Unfortunately many commercial routines, besides the obvious geometry overlay, only present the function values as a linear sequence of node values and don't allow the user to select cuts. Additional capabilities as contour mapping and pseudo-colour mapping are most welcome.

- Computation of function derivatives (and visualization). Sometimes only the function is computed, and the user is interested in some special derivatives of the function, as when heat fluxes are needed, besides temperatures.
- Feedback on the meshing, refining it if there are large gradients, or large residues in the overall thermal balance. It is without saying that the user should do all the initial trials (what usually takes the largest share of the effort) with a coarse mesh, to shorten the feedback period.
- Precision and sensitivity analysis by running some trivial cases (e.g. relaxing some boundary condition) and by running 'what-if' type of trials, changing some material property, boundary condition and even the geometry. Eventually, some the numerical simulation results must be validated against experimental tests.

A global checking, showing that the detailed solution verifies the global energy equation, gives confidence in 'black box' outputs and serves to quantify the order of magnitude of the approximation.

Spacecraft thermal testing

Measurement is the ultimate validation of real behaviour of a physical system. But tests are expensive, not only on the financial budget but on time demanded and other precious resources as qualified personnel. As a trade-off, mathematical models are developed to provide multi-parametric behaviour, with the hope that, if a few predictions are checked against physical tests, the model is validated to be reliable to predict the many other situations not actually tested.

Thermal tests can be performed at component, subsystem, or system level. Although tests should be carried out with maximum fidelity to expected operational procedures and realistic space environment (notably vacuum), sometimes, preliminary tests are performed at room pressure, like temperature cycling and operational sequences (e.g. turn-on and turn-off active components), but thermal vacuum tests are needed at the end. Main parameters of thermal cycling are temperature extremes, number of cycles, and rate of temperature change. Care must be paid to the thermal distortions caused by the ground-test-equipment used to support the flight components in the test facility. At the spacecraft level, thermal balance tests are performed to verify the thermal control system and global thermal analysis.

Qualification tests are performed to validate all the steps in the design and manufacturing process, from requirements to testing techniques (tooling, handling procedures, personnel expertise...). Hardware for thermal qualification is subjected to more severe tests than flight hardware (i.e. to cold and hot thermal environments beyond those expected in flight), to demonstrate that a safety margin exists), although both are to be manufactured to the same standards. Flight hardware and spares are only subjected to milder acceptance tests.

Final testing of a large spacecraft for acceptance as a delivered product is at the present limit of technology, since very large vacuum chambers, with a powerful collimated solar-like beam, and walls kept at cryogenic temperatures, must be provided (and the spacecraft able to be deployed, and rotated in all directions, while measuring).

Typical temperature discrepancy between the most advanced numerical simulation and the most expensive experimental tests may be some 2 K for most delicate components in integrated spacecraft (much lower when components are separately tested).

[Back to Spacecraft Thermal Control](#)